Submarine morphology of the Comoros volcanic archipelago

A. Tzevahirtzian, S. Zaragosi, P. Bachèlery, L. Biscara, E. Marchès

Submarine morphology of the Comoros volcanic archipelago.

Tzevahirtzian A. [a, b*], Zaragosi S. [b], Bachèlery P. [c], Biscara L. [d], Marchès E. [d]

[a] Dipartimento di Scienze della Terra e del Mare (DiSTeM), Università degli Studi di Palermo, via Archirafi 20-22, 90123, Palermo, Italy.

[b] EPOC, UMR CNRS 5805, Université de Bordeaux, allée Geoffroy Saint-Hilaire, CS 50023, F-33615 Pessac cedex, France.

[c] Université Clermont Auvergne, CNRS, IRD, OPGC, Laboratoire Magmas et Volcans, 6 avenue Blaise Pascal, 63178 Aubière, France.

[d] SHOM, 13 rue du Chatellier, CS 92803, F-29228 Brest cedex 2, France.

[*]corresponding author: athina.tzevahirtzian@unipa.it

Abstract

A detailed morpho-bathymetric study of the Comoros archipelago, based on mostly unpublished bathymetric data, provides a first glimpse into the submarine section of these islands. It offers a complete view of the distribution of volcanic structures around the archipelago, allowing to discuss the origin and evolution of this volcanism. Numerous volcanic cones and erosional-depositional features have been recognized throughout the archipelago. The magmatic supply is focused below one or several volcanoes for each island, but is also controlled by lithospheric fractures evidenced by volcanic ridges, oriented along the supposed Lwandle-Somali plate boundary. Massive mass-wasting morphologies also mark the submarine flanks of each island. Finally, the submarine geomorphological analysis made possible to propose a new scheme for the

succession of the island's growth, diverging from the east-west evolution previously described in the literature.

Keywords: Comoros archipelago, morpho-bathymetry, submarine volcanism, volcanic ridges, volcanic cones, mounds, mass slope instabilities.

1. Introduction

From the ocean floor to their top, oceanic hot spot islands form very large reliefs and can be considered as the largest mountains on Earth (Huff and Owen, 2013). Their morphology results from the juxtaposition of both endogenous (mantle and crustal geodynamic and tectonic, melt generation and differentiation, intrusive growth…) and exogenous (eruptive regime and dynamism, gravitational instabilities, erosion, sediment transport, weathering…) processes, and consequently provides good insights into how oceanic islands grow and evolve (Bachèlery and Villeneuve, 2013). The submarine flanks of these edifices, by far larger than their emerged counterpart, remain however less studied given the difficulties inherent to their observation and the costly resources to be deployed. Since pioneering work (Moore, 1964; Moore and Fiske, 1969; Spiess et al., 1969), significant progress has been made in mapping the submarine slopes of oceanic volcanoes and understanding their development. They are shaped by two main groups of processes: growth by primary volcanic emissions (lava flows, pyroclastics, hyaloclastites) and intrusions, and destruction by gravity-driven instabilities (landslides, slumps, catastrophic debris avalanches, density flows) and shallow-water erosion (waves, sea-level changes, heavy rains) (e.g., Holcomb and

Searle, 1991; Ramalho et al., 2013; Saint-Ange et al., 2013; Staudigel and Koppers, 2015; Casalbore, 2018). Primary volcanic structures most often reflect the interactions between magmatism and tectonics (Binard et al., 1992; Hekinian et al., 2003; Devey et al., 2003; Rubin et al., 2012) and the degree of maturity of the volcano (Mitchell, 2001; Acosta et al., 2003; Casalbore et al., 2015; Clague et al., 2019). As such, the morpho-structural analysis of volcanic edifices can provide insights for evaluating local geodynamics and volcano's evolutions.

Gravity-driven instabilities have been recognized as a common process in the building of oceanic islands, including many basaltic intraplate volcanoes. Two main types of landslides are generally covering large portions of the volcanoes' submarine flanks: catastrophic debris avalanches (fast-moving landslides) and more coherent slumps (Moore et al., 1989; McGuire, 1996; Krastel et al., 2001a; Masson et al., 2002; Mitchell et al., 2002; Coombs et al. 2004; Masson et al., 2008; Oehler et al., 2008; Le Friant et al., 2011; Mitchell et al., 2013; Denlinger and Morgan, 2014; Hunt and Jarvis, 2017). Erosion forms gullies and canyons, and feed fan-shaped turbidite deposits that may widely spread on the abyssal plain (Krastel et al., 2001b; Sisavath et al., 2011; Mazuel et al., 2016). As volcanic activity declines, the combined effects of erosion and subsidence reduce the height of the volcanic edifice and led to the formation of an insular shelf (Quartau et al., 2014; Romagnoli et al., 2018). In tropical environment, the growth of carbonate submarine terraces may give information on the chronological evolution of the islands (Puga-Bernabéu et al., 2016; Counts el al., 2018).

In comparison to other volcanic archipelagoes, such as Hawaii, Canaries or Azores, Comoros Islands are poorly known, and the seabed of the region is very little studied yet. This is an obstacle in the comprehension of the origin of the Comorian volcanism, which explains the open debate for 50 years. The Comoros Islands display the different

71 erosional stages specific to volcanic dynamic (Darwin, 1842). The islands have been
72 almost exclusively studied in their terrestrial part, except for Mayotte due to its lagoon
73 and its developed barrier reef (Guilcher et al., 1965; Zinke et al., 2003a & b; Audru et
74 al., 2006). Studies on the geology, geochronology and the archipelago's volcanism
75 have been made, but many questions remain to be resolved (Esson et al., 1970;
76 Hajash and Armstrong, 1972; Emerick and Duncan, 1982; Nougier et al., 1986;
77 Bachèlery and Coudray, 1993; Späth et al., 1996; Michon, 2016).

78 This paper aims to document the geomorphology of the submarine part of the Comoros
79 archipelago, emphasizing the juxtaposition of erosive-depositional and volcanic
80 structures. Based on our morphological analysis, the origin and evolution of the
81 Comoros archipelago are discussed.

82

83 ## 2. Geological background

84 ### 2.1. Regional context of volcanism

85 The Comoros archipelago includes the islands of Grande Comore, Anjouan,
86 Mohéli and Mayotte, extending over 270 km in the Somali-Comoros Basin, at the
87 northern entrance of the Mozambique Channel in the western Indian Ocean (Fig.1A,
88 B).

89 The Comoros volcanic edifices stand on a tectonically and seismically active zone,
90 extending approximately E-W, from the northern end of the Davie Ridge to the north of
91 Madagascar (Fig.1A). It is considered as the potential diffuse Lwandle-Somali sub-
92 plate boundary (Rindraharisaona et al. 2013; Michon, 2016; Stamps et al., 2018; Famin
93 et al., 2020), and part of the SE seaward extension of the East African Rift System

94 (Kusky et al., 2010; Franke et al., 2015; Deville et al., 2018; Courgeon et al., 2018;
95 O'Connor et al., 2019).

96 From the Jurassic to Early Cretaceous, the Gondwana breakup was marked by
97 NE-SW oriented seafloor ridges allowing the gradual opening of Somali and
98 Mozambique basins, and the southern migration of Madagascar (Segoufin and Patriat,
99 1980; Coffin and Rabinowitz, 1987; Key et al., 2008; Emmel et al., 2011; Davis et al.,
100 2016; Mueller and Jokat, 2019; Thompson et al., 2019). During the Cenozoic, the East
101 African Rift System develops in two major branches (Malod et al., 1991; Mpanda, 1997;
102 Chorowicz, 2005; Franke et al., 2015), and extends offshore from the Miocene and
103 then the Pliocene (Mougenot et al., 1986; Franke et al., 2015; Macgregor, 2015).
104 Several submarine grabens characterize the offshore branch of the rift and a major
105 structural high, the Davie Ridge (Raillard, 1990; Chorowicz, 2005; see also Franke et
106 al., 2015, Fig.1). Since the Pleistocene, this offshore branch extends southwards
107 through the reactivation of the Davie Ridge in the southern part of the Sakalaves
108 Seamounts and possibly up to the Quathlamba Seismic Axis (Franke et al., 2015;
109 Courgeon et al., 2018).

110 The volcanic activity of the Comoros Islands began since the Mio-Pliocene (Esson
111 et al., 1970; Hajash and Armstrong, 1972; Emerick and Duncan, 1982; Pelleter et al.,
112 2014). Only few absolute ages are available in the literature, obtained from the
113 emerged part of each island: Mayotte 10.6 ± 0.5 Ma to ~6 ka, Anjouan and Mohéli 11.1
114 ± 0.5 Ma to 0.36 ± 0.09 Ma and 5.0 ± 0.4 Ma to 0.48 ± 0.15 Ma, respectively, and
115 Grande Comore 0.13 ± 0.02 Ma to present (Hajash and Armstrong 1972; Emerick and
116 Duncan, 1982; Nougier et al. 1986; Zinke et al., 2003a, 2005; Debeuf, 2004; Pelleter et
117 al., 2014). Nougier et al. (1986) estimated the onset of the volcanism of Mayotte
118 around 15-10 Ma, but according to Michon (2016), the volcanic activity of the Comoros

119 archipelago is probably older and would have started in Mayotte 20 Ma ago, and then
120 developed in Anjouan, Mohéli and Grande Comore almost simultaneously 10 Ma ago.
121 From seismic stratigraphy, Leroux et al. (2020) confirm that the main volcanic phase of
122 Mayotte occurred between ~15-20 Ma and ~3 Ma. Today's active volcanism has been
123 described for the island of Grande Comore and offshore Mayotte. On Grande Comore,
124 Karthala's volcano most recent eruptions occurred in 1991, and from 2005 to 2007
125 (Bachèlery et al., 1995; Bachèlery et al., 2016). A seismic crisis and a submarine
126 volcanic eruption began 50 km east of Mayotte in mid-May 2018. Activity is ongoing at
127 the time of writing (Feuillet et al., 2019; Lemoine et al., 2020; Cesca et al., 2020).

128 The Comoros volcanism has been interpreted in different ways. It was regarded
129 as hotspot-related (Emerick and Duncan, 1982; Emerick, 1985; Hajash and Armstrong,
130 1972; Morgan, 1972; Späth et al. 1996; Class et al., 1998) or due to deep lithospheric
131 faults (Upton, 1982; Nougier et al., 1986), in relation to the East African Rift System
132 (Michon, 2016; O'Connor et al., 2019; Famin et al., 2020). The most recent work tends
133 to consider the Comoros archipelago as an E-W right-lateral shear zone and a diffuse
134 boundary between the Lwandle and Somali plates, rather than the surface expression
135 of a deep mantle plume (Michon, 2016; Famin et al, 2020).
136

137 **2.2. Geological framework of the islands**

138 Grande Comore (Fig.2) is the largest island (1,100 km^2) of the Comoros
139 archipelago. Three volcanic massifs shape the island (Bachèlery and Coudray, 1993;
140 Bachèlery et al., 2016). Karthala (2,360 m) is a frequently active shield volcano. On the
141 northern part of the island, La Grille Massif was mostly active during the Pleistocene
142 (Bachèlery and Coudray, 1993; Bourhane et al., 2016) and has erupted several times

143 in the last few thousand years (1300 ± 65 years BP and 740 ± 130 years BP in
144 Bachèlery and Coudray, 1993; Bachèlery et al., 2016). Unusual steep slopes (locally
145 >30°) on Karthala and La Grille flanks have been interpreted as landslide scars
146 (Bachèlery et al., 2016). Recent eruptive fissures and cinder cones observed on
147 Karthala and La Grille volcanoes define volcanic rift zones with N-S and NW-SE
148 orientations (Fig. 2A - Bachèlery et al., 2016). M'Badjini Massif is considered to be the
149 oldest volcanic center of Grande Comore (Bachèlery and Coudray, 1993). A
150 discontinuous fringing reef is present all around the coastline of Grande Comore
151 (Guilcher et al., 1965).

152 Mohéli (Fig.3) is the smallest island of the Comoros archipelago (290 km^2)
153 culminating at Mount M'Ze Koukoulé (790 m). Little is known about the geology of
154 Mohéli. Nougier et al. (1986) proposed the existence of ancient series outcropping
155 mainly in the west of the island, while the summits and the east of the island are
156 covered by younger formations. Recent craters and lava flows define a WNW-ESE (N
157 115°) alignment that may correspond to an old volcanic rift zone (see Fig.4 in Famin et
158 al., 2020). A well-developed fringing reef is present all around the island (Guilcher et
159 al., 1965).

160 Anjouan (Fig.4) has a triangular shape of 424 km^2, with three peninsulas extending
161 to the north, south and west. Esson et al. (1970) suggest that NW-SE and NNW-SSE
162 oriented faults probably control its fairly rectilinear coastlines, while its northern
163 concave-shaped coastline is associated with faults and local subsidence phenomena.
164 The relief of Anjouan is very rugged and shaped by deep river erosion of the oldest
165 basaltic sequences, with its highest peak, Mount N'Tingui, culminating at 1,575 m
166 (Esson et al., 1970). The oldest formations are mainly outcropping in the center of the
167 island, while the peninsulas are covered with more recent series (Nougier et al., 1986;

Famin et al., 2020). Well-preserved volcanic cones, corresponding to recent eruptions, form alignments (N105° and N152°) that roughly correspond to the main topographic crests of the island (see Fig. 4 in Famin et al., 2020). These alignments are interpreted as volcanic rift zones. The island is bordered by fringing reefs on two-thirds of its periphery (Guilcher et al., 1965).

Mayotte (Fig.5) consists of two main islands, Grande Terre and Petite Terre, and nearly 20 smaller islets (Guilcher et al., 1965). A unique mountain range and secondary massifs with steep slopes and narrow coastal plains mark its topography (Lachassagne et al., 2014). Mayotte is considered to be the result of subaerial volcanic activity since about 10 Ma, with at least two Miocene to Pleistocene shield volcanoes (Southern complex and Northern complexes) on which more recent massifs (Digo and M'Tsapéré) have been built (Audru et al., 2006; Debeuf, 2011; Nehlig et al., 2013; Lacquement et al., 2013; Pelleter at al., 2014; Vittecoq et al., 2014). Audru et al. (2006) described normal faults along two main directions: N45° and N160-180°. Dykes are essentially observed along the northwestern coast with a dominant N150-160° orientation (Famin et al., 2020). No clear rift zone can be identified. During the last 20,000 yrs (Last Glacial Maximum), the island has undergone a subsidence of 2.4 - 5 m (Camoin et al., 1998; Camoin et al., 2004), which corresponds to an average subsidence rate of 0.19 to 0.25 mm/year (Audru et al., 2006; Montaggioni & Martin-Garin, 2020). Mayotte has the largest barrier reef - lagoon complex in the Indian Ocean (Zinke et al., 2003a & b). The thick soils resulting from the laterite alteration of basaltic lavas (Guilcher et al., 1965), and the coastal indentations of the island linked to erosion, are also indicative of Mayotte's maturity.

3. Material and methods

193 **3.1. Multibeam bathymetry and seismic data**

194 Since 2004, several oceanographic surveys carried out by the French Hydrographic
195 Office (Shom) and the French Geological Survey (BRGM) have enabled the acquisition
196 of data necessary for this study (more than 13,000 km of multibeam bathymetric data
197 and sub-bottom seismic lines, available on data.shom.fr). Five bathymetric Digital
198 Elevation Models (DEMs) at a resolution ranging from 1 m near the shores (<30 m
199 water depths) to 100 m in the deep sea (>30 m to 3,500 m water depths) covering the
200 Comoros Archipelago were provided by the Shom. In shallow waters, the bathymetric
201 DEMs are generated through Lidar surveys conducted under the Litto3D® program
202 (Shom – IGN). Multibeam bathymetry data and sub-bottom seismic lines were collected
203 by the Shom essentially on RV *Beautemps-Beaupré* and in the framework of
204 collaborations (e.g. BATHYMAY cruise acquired by BRGM on the R/V *Marion*
205 *Dufresne*). In addition, external data were also gathered in order to complete the
206 bathymetric coverage of the study area: soundings and isobaths of electronic chart of
207 navigation (ENC) and GEBCO 2014 bathymetric grid. The bathymetric DEMs were
208 subsequently harmonized and gridded into a similar resolution – 100 m - (WGS84
209 World Mercator) following the method described by Biscara et al. (2016). From this
210 DEM and using ArcGis v10 software, a morpho-bathymetric analysis was performed:
211 geomorphological analysis were made by means of slope, hillshade, 2D and 3D views.
212
213 The sub-bottom seismic lines were collected during the Shom 2009 - 2010 campaigns
214 with a Simrad SBP 120 sediment sounder (CHIRP). It has a modulating acquisition
215 frequency between 2.5 and 7 kHz and provides a maximum vertical resolution of ~20
216 cm. This makes possible to characterize the acoustic properties of shallow sub-
217 seafloor. Seismic data were processed with The Kingdom © software, two-way travel

218 times (TWT) have been converted in meters using an average seismic velocity of 1500
219 $m.s^{-1}$.

220

221 **3.2. Limits of the study**

222 Data resolution does not allow a precise identification of the morphology of some
223 volcanic and sedimentological features existing all around the Comoros archipelago.
224 Concerning volcanic cones, we are unable to identify reliefs of less than 20 m high.
225 Even for higher landforms, it is sometimes difficult to clearly differentiate volcanic cones
226 from large debris or megablocks. Moreover, the lack of multibeam data in some parts
227 of the archipelago, does not always allow us to accurately characterize the
228 morphologies observed in some submarine portion of the islands, such as the insular
229 shelf, volcanic cones or bedforms.

230 The lack of both seismic profiles and cores/grab sediment sampler, in order to better
231 understand the internal morphologies and to develop the sedimentological and
232 stratigraphic evidences on the shelves and the flanks of the Comoros islands,
233 respectively, prevents further interpretation of the various structures observed from the
234 bathymetric data. The scarcity of previous work, and in particular the lack of
235 geochronological data, often forces us to a merely morphological interpretation. This is
236 for example the case for the terraces. Since those of Mohéli have never been studied,
237 a detailed comparison with those of Mayotte is impossible.

238

239 **3.3. Terminology**

240 **Pointy cones, flat-topped cones, mounds**

241 Volcanic cones and mounds are common features around volcanic archipelagoes.
242 Here, volcanic cones mostly correspond to reliefs with an overall conical “pointy” shape
243 (Fig.6, 7C). Pointy cones have a base varying from circular to elliptical, and smooth
244 flanks with gradients ranging between 15° and 30°, defined as large hyperbolas on
245 seismic profiles (ET3 on Fig.8A, B). They are most often isolated (Fig.6B to G), but can
246 also be aligned and coalescent, constituting alignment of volcanic cones (Fig.6C to F).
247 A few flat cones have been identified, mainly at great depths (>1,700 m) around
248 Vailheu Bank (Fig.6F). They have simple, circular to slightly elongated shapes, but their
249 flat and irregular top distinguishes them from pointed cones (Fig.7D). They have an
250 average basal diameters of 2,200 m and an average height of 400 m, smooth flanks
251 with gradients ranging between 30° and 40°.
252 Mounds are low relief, sub-circular or sometimes irregular in shape (Fig.6C, 7B). They
253 show an average surface of 15 km^2 (basal diameter ranging from 2,000 to 8,500 m)
254 and an average height of 80 m. They are often isolated (as it is the case in the north of
255 the archipelago, Fig.6C). Small-scale faulting along the summit and the flanks of the
256 mounds and forced folds near the base are visible on the seismic profile (ET2 on
257 Fig.8A, B).
258 Other volcanic structures like small volcanic linear ridges or linear fissure eruptions,
259 thick lava flows, are probably present and may be suspected in some places (i.e. east
260 of Mayotte or east of Anjouan). However, the too low resolution of our DEM does not
261 allow defining them precisely. Therefore, they were not taken into account in this study.
262
263 **Megablocks**
264 The existence of megablocks associated with debris avalanche deposits is strongly
265 suspected. Examples of reliefs with irregular morphology, a few tens to hundred meters

high, identifiable as megablocks, are recognizable, for example south of Grande Comore (Fig.6G) or north of Anjouan (Fig.6D). However, the too low resolution of the DEM does not allow us to characterize them precisely, and their distinction from volcanic cones is often very tricky. So, it seems unreasonable to us to try to point them out specifically.

Terraces and insular shelves

An insular shelf and two submerged terraces surround Mohéli and Mayotte, as shown on Fig.3, 5, 6A and B. The presence of these features is an important indicator of sea level changes and/or land subsidence (Quartau et al., 2010; Ramalho et al., 2013). Such features are generally well developed when erosion dominates volcanism. Unfortunately, as explained in section 3.2, in our case these data cannot be used beyond morphological analyzes.

Channel and gullies

Channels and gullies are shown on Fig. 6A, 6B and 6G. Channels surround the islands and may originate in the upper slope, continuing downslope to the basin floor (Fig.6B, G). In places, gullies are present in the uppermost slopes or mid-slopes, when incision is not deep or narrow enough to form channels (Fig.6A).

Bedforms

'Wave-like' bedforms are present on the flank of the Comoros Islands (Fig.6B, F and Fig.9). They have an average wavelength of 2 km and a wave height ranging between 15-130 m according to the islands. They cover at least an area of 4,000 km^2, which make them an important feature of the study area. Bedforms correspond to small

geomorphic features and are useful for the understanding of the transfer of material from subaerial to deeper marine flanks. Insights are given on the size distribution, the morphology and the genesis of bedforms observed around the submarine volcanic flanks of the islands. These deformed synsedimentary deposits can be generated by gravity instabilities or/and by sediment-laden gravity (Correggiari et al., 2001; Lee et al., 2002; Mulder, 2011; Casalbore et al., 2020).

4. Results

Table 1

4.1 Grande Comore

Grande Comore's volcanic edifice has an elongated shape, with an N-S orientation (Fig.1B, 2A). It is extended by three volcanic ridges (VR) characterized by high bathymetry and a high density of volcanic cones, west of Vailheu Bank (VR1), between Grande Comore and Vailheu Bank (VR2), and south of Grande Comore connecting Mohéli (VR3, Fig.1C). These volcanic ridges are elongated, steep-sided reliefs. Many isolated cones or alignments of volcanic cones are identifiable along the volcanic ridges, and on the submarine flanks of the island. They are present all around the island (average density of 0.3 cone/km^2), but their distribution is not uniform. Two subcircular mounds located in the southwest of the island (average height 40 m, radius 1.5 km) have been identified (Fig.2A).

West of Grande Comore, the Vailheu Bank is a 9 km^2 submarine terrace exposed occasionally at low tide, with very steep slopes (47 to 50°) near its top (Fig.2D). Vailheu

315 Bank is located at the extremity of VR2, 20 km west off the coast of Karthala volcano
316 (Fig.2A and C). The VR2 ridge (N65°) starts close to the west coast of Grande Comore.
317 Its depth increases regularly (mean slope gradient <4°) to reach a water depth of about
318 1,100 m near the base of the Vailheu Bank (Fig.10A, line 2). The western flank of the
319 Vailheu Bank reaches a depth of 2,700 m. Northeast and east of the Vailheu Bank, the
320 submarine slopes gradually decrease without significant escarpment, reaching 1,500 m
321 below sea level (bsl). West of the Vailheu Bank, a high density of volcanic cones
322 seems to outline a general N-S to NE-SW oriented alignment (N20°) rising to >1,000 m
323 above the surrounding seafloor (VR1). In detail, some alignments of cones seem to be
324 oriented radially with respect to the Vailheu Bank, while others are more or less N-S.
325 Unfortunately, the lack of data west of this ridge does not allow its precise description.
326 The tallest volcanic cone of this study (657 m high) is located about 18 km SW of the
327 Vailheu Bank.

328 South of Grande Comore, the southeast Karthala rift zone extends offshore up to 13
329 km from the coast by a topographic ridge about 15 km wide with a gentle slope (~ 4° -
330 Fig.10A, line 1). It connects to the volcanic ridge VR3 (N160°) located at a mean water
331 depth of 900 m, the deepest part of the ridge being about 1,080 m bsl (Fig.1B, C & 2A).
332 This ridge is connected to Mohéli's edifice with a steep slope (> 30° - Fig.10A, line 1).

333 Submarine slopes of Grande Comore are generally steeper than subaerial slopes (Fig.
334 2D). Areas with rugged morphology and numerous volcanic cones can be distinguished
335 in the submarine morphology, such as, for example, north of La Grille volcano and east
336 of M'Badjini Massif (lines 3 and 5, respectively, on Fig. 10A). In contrast, only few
337 volcanic cones are visible along the southeastern submarine slopes of La Grille Massif,
338 where a smooth morphology is identifiable despite the limited data available in this
339 area. Southwest of Karthala volcano, in a sector bounded by the volcanic ridges

340 VR1/VR2 and VR3, a bathymetric bulge corresponds to a large area of blocky surface
341 morphology (Fig. 2A, 6G, 7A & E). In this area, the mean slope decreases from >30° to
342 <3° from 1,000 m to 3,000 m bsl (line 1 on Fig.10B), with less irregularity compared, for
343 example, to the uneven slopes observed north of La Grille Massif. These fan-shaped
344 deposits extend widely on the abyssal plain, to at least 45 km from the coast (Fig. 2A).
345 They are dissected and bound by channels up to 100 m deep (Fig. 7E).

346 A number of channels, rectilinear in shape, surround submarine slopes of Grande
347 Comore (Fig.2A). Only one major channel (GC1) has been identified east of the island.
348 CG1 is located northeast of M'Badjini Massif and extends in continuity with one of the
349 major landslide of the eastern flank of Karthala volcano (see Bachèlery and Coudray,
350 1993). Its southern edge corresponds to the continuation of a scarp identified on land.
351 The widest channel (GC2) is located in the southern part of the island and is 46 km
352 long and 3 km wide, originating from a spectacular landslide amphitheater affecting the
353 southern flank of Karthala. Other significant channels, around 20 km long and 2 km
354 wide, can be identified around Grande Comore (Fig.2A): mainly to the southwest (GC3,
355 GC4 and GC5), separated by interfluves with irregular blocky surfaces, and north
356 (GC6, GC7, GC8) separated by interfluves that may represent preserved portions of
357 the submarine flanks, formed through alignments of volcanic cones and possibly the
358 superimposition of lava flows and other volcanic products (Fig.2B). Channels are also
359 present north and west of the Vailheu Bank but are smaller in size (3 to 11 km long and
360 1 km wide).

361 Bedforms are present, especially on the northwestern submarine flanks (profile 'd-e' in
362 Fig.2A, Fig.6F, Fig.9). The range of bedforms wavelengths and wave heights is 1 to 2.7
363 km and 25 to 45 m, respectively, for a slope gradient of 2.5° (slope gradients varying in
364 average between 8.3° and 0.3° - Fig.9). No clear evolution of the bedform

365 morphologies is observed through depth. However, bedforms are also identified south
366 of Grande Comore and perpendicular to VR3 (profile 'g-f' in Fig.2A, Fig.9). Between
367 2,600 and 2,900 m bsl, bedforms are significant with a maximum wavelength and
368 height of 1.1 km and 50 m, respectively, and highest slopes of 17° (Fig.9). Their size
369 decreases below 2,900 m: respectively, 0.7 km and 10 m and an average slope of 6°.
370 Grande Comore seems to have a single, little developed insular shelf with an edge
371 located around 100 m water depth. Unfortunately, bathymetric data are missing at
372 shallow depth, which unable the possibility for further descriptions of the insular shelf.
373

374 **4.2 Mohéli**

375 Mohéli is located at the junction of two elongated volcanic ridges, VR3 already
376 described, originating from Grande Comore, and VR4, at an average depth of 1,700 m,
377 connecting Mohéli and Anjouan (Fig.1D, 3A). The orientation of VR4 (N55°) is almost
378 parallel to VR2 connecting Grande Comore to the Vailheu Bank (N65°). Volcanic cones
379 are identifiable on the two volcanic ridges VR3 and VR4 (Fig.3C). Mohéli's volcanic
380 edifice has an approximately rectangular shape, with two large amphitheaters affecting
381 its southern flank. The flanks east, southeast and southwest of Mohéli (respectively
382 lines 8, 9 and 10 on Fig. 10A) are irregular, with slope gradients mainly ranging from
383 14° to 5°. They are incised by small channels (8 to 10 km long, ~1 km wide). The
384 density of volcanic cones appears to be low (around 0.1 volcanic cones per km^2).
385 Several large volcanic cones can be identified on the rugged terrain east of Mohéli (Fig.
386 3A and line 8 in Fig.10A), in line with the general orientation of the island and following
387 the alignment of the most recent cones recognized ashore. This may be the offshore
388 extension of the old Mohéli volcanic rift zone.

While the northern and western submarine flanks of Mohéli are characterized by very steep and smooth upper slope surfaces, two huge amphitheatre-like depressions that open downslope, and a fan-shaped bathymetric bulge with chaotic terrains, characterize the area south of Mohéli (Fig.3A). In this area, networks of tributary channels coalesce to form three large channeled systems (Mo1, Mo2, Mo3). Mo1 is the largest channel of 60 km long and 2 km wide. These channels have interfluves shaped by the chaotic terrains, on which we can identify bedforms and volcanic cones and/or megablocks (Fig.3A, D). Unfortunately, multibeam data are missing south of Mohéli to fully describe this southern flank. Available data show bedforms reaching 3,500 m depth, more than 70 km from the island. Bedform in the southeast of Mohéli (profile 'g-h' in Fig.3A and Fig.9) have wavelengths and wave heights ranging from 1.3 to 2.2 km and 50 to 80 m, respectively. Slope gradient varies from 12.5° to 0.1°, with an average value of 4°. Between 2,700-2,800 m bsl, the bedform wavelength is higher than in the deeper section of the flank. In the eastern flank of Mohéli, south VR4, bedforms are located at a water depth ranging from 3,130 and 3,500 m (profile 'i-j' in Fig.3A and Fig.9). The range of bedform wavelengths and wave heights is, respectively, 1.2 to 2.2 km and 15 to 55 m (average slope gradient 2°, Fig.9). The highest average slope gradient is 7° and the lowest 0.1°, but no clear evolution of the morphologies is observed through depth.

An insular shelf and two submarine terraces developed around Mohéli. The insular shelf T1Moh is large with a broadly rectangular shape and a surface area of 987 km^2, and a shelf break located at 0-100 m bsl (Fig.3A). The submarine terraces T2Moh, to the southwest of Mohéli, and T3Moh, to the northeast and east, are located at ~600 m bsl (Fig.3A), with a surface area of 52 km^2 and 112 km^2, respectively. Numerous small landslide scars affect T1Moh (Fig.3B). The slopes that connect T1Moh to T2Moh and

414 T3Moh vary from 25 to 40°. From the edge of T1Moh, the slope is very steep, dipping
415 up to 45°, then decreasing offshore to a depth of 2,500 m in the north and 1,500-2,000
416 m in the south (profile 'a-b' on Fig.3D).

417

418 **4.3 Anjouan**

419 The three peninsulas shaping the island of Anjouan extend underwater with rugged
420 slopes (Fig. 4). The south volcanic rift zone (N152°) extends more than 18 km offshore
421 toward the south, while the northern peninsula shows a submarine extension of 16 km.
422 The submarine extension of the western peninsula forms a 90° angle, with respect to
423 the orientation of the subaerial part, to connect Mohéli by a volcanic ridge (VR4 -
424 Fig.4A). Many volcanic cones are identifiable along and near these ridges. East of the
425 island, isolated volcanic cones and volcanic cone alignments are more densely
426 concentrated on the middle part of the eastern flank. This corresponds to a positive
427 morphology (more than 1,000 m above the surrounding seafloor) between Anjouan and
428 Mayotte (Fig.1E and profile 'd-e' in Fig.4A). It suggests the existence of a submarine
429 ridge of NW-SE orientation towards Mayotte (VR5 - N130°). Some structures in this
430 area form small linear ridges visible over several kilometers. Given the resolution of our
431 DEM, it is difficult to interpret it (see 3.3). The density of cones is estimated between
432 0.1 to 0.3 volcanic cones per km^2 according to the area.

433 The northern and southwestern flanks show broad embayments, and steep and
434 smooth concave upper slopes. On the lower slopes, an area with irregular blocky
435 topography extends over several tens of kilometers (Fig.4A, B, Fig.6D). Large channels
436 have formed, with three major channels (Anj1, Anj2 and Anj3) located on the
437 southwestern flank, (16 to 23 km long and 1 to 2 km wide). Northeast and south of

Anjouan, smaller channels (10 km long and 1.5 km wide) have also developed (Anj4, 5, 6 and 7 - Fig.4A).

Anjouan has a single, little developed insular shelf, with steep upper slopes from the shelf break (40° on the northwest and southwest of the island and 35° in the east) gradually decreasing downslope (4°) reaching a depth of 3,000 m (Fig.4A, B).

4.4 Mayotte

The submarine morphology of Mayotte reflects the onland geological framework of the island with a NW-SE elongation for the northern part of the island, and a semi-circular morphology in the south (Fig.5A). Volcanic cones are scattered around Mayotte. Their density is low (max 0.1 volcanic cones per km^2), except for two areas in the northwest of the island towards Anjouan (VR5, previously described), and towards the east where a WNW-ESE oriented volcanic ridge (N120°, VR6), extending from the recent volcanism of Petite Terre to about 3,500 m bsl, is clearly visible (0.2 cones per km^2). This ridge is the site of the current seismicity and ongoing volcanic eruption (Fig. 5). One of the tallest volcanic cones in the study area (520 m high) is located on this ridge, close to the current eruptive center that is more than 800 m high (Feuillet et al., 2019).
On the western and southern flanks of the island, the submarine slopes show a slightly concave shape and a chaotic surface with many undulations (Fig.5A, D). Submarine channels are homogeneously present on all of the flanks, from the base of the reef plateau to the base of the edifice. These channels are radial to Mayotte but their morphology is mostly sinusoidal (see Audru et al., 2006 for more details - Fig. 5A). A fan-shaped field is formed by a series of channels and interfluves. Between the channels, bedforms were recognized all around the island and are present between

1,500-2,700 m bsl (Fig.6B). The range of bedforms wavelengths and wave heights is 1 to 2 km and 40 to 130 m, respectively (profile 'k-l' in Fig.5A and Fig.9). They are crescentic and the average slope gradient is 6°. The largest bedforms occur between 2,150 and 2,700 m bsl. Bedforms also occur in the bed of the channels (profile 'm-n' in Fig.5 and Fig.9) with a range of wavelengths and wave heights of 1 to 1,7 km and 25 to 40 m, respectively. They are crescentic downslope and have an average slope gradient of the bedforms is 3.5° (Fig.9). At 3,250 m of water depth, bedforms are more pronounced with a slope gradient up to 10°.

An insular shelf and two submarine terraces have been previously identified (see Audru et al., 2006). Mayotte's insular shelf T1May is the largest of the Comoros archipelago (1,860 km^2). A lagoon has been formed with an almost continuous reef barrier, and with the insular shelf edge located at 0-50 m water depths. Channels and karst systems (150 m bsl) are visible on the insular shelf (Audru et al., 2006 – Fig.5). Two small terraces (Fig. 5A) are located in the northwest of Mayotte (T2May) at 450 - 600 m bsl (area of 123 km^2), and in the southwest of Mayotte (T3May) at a depth varying from 450 to 830 m bsl (area of 291 km^2). Each terrace is delimited on its upper and lower edges by steep slopes, and its top slopes gently down (2 - 4° - Fig. 5D and line 11 in Fig.10A). Several landslide scars affect the terrace T1May (Fig.5C). This is particularly obvious in the southeast where T1May shows a clear amphitheater-shaped landslide scar, with concave slopes lower down (Fig. 5A and line 6 on Fig.10B). On the terraces T2May and T3May, collapsed debris deposits can be observed (Fig.5C, D). The slopes that connect T1May to T2May and T3May vary from 40 to 45°, decreasing offshore with slightly concave gentle slopes (5°).

4.5 The Jumelles ridges

Northeast of Mayotte, two NW-SE (N140°) parallel submarine ridges (VR7 and VR8), named the Jumelles, form isolated reliefs elevating as much as 2,160 m above the seafloor (Table 1, Fig.1B, F). The Jumelles correspond to elongated landforms, with relatively rough slopes, and numerous volcanic cones and alignments of volcanic cones (Fig. 5B, 8C). The density of volcanic cones is high with 0.2 cones per km^2. One of the tallest volcanic cones of this study (538 m high) is located south of the Jumelles.The two ridges differ in size and elevation. The western ridge (VR7) is 46 km long, 15 km wide and 2,200 m high, whereas the eastern one (VR8) is 35 km long, 10 km wide and 1,500 m high. No submarine channels or chaotic terrains are present. At the northern end of VR8, a group of volcanic cones seems to be aligned along an ENE-WSW orientation (N70°), close to that found for the ridges VR2 (between Karthala and Vailheu Bank) or VR4 (Anjouan and Mohéli). This alignment appears to extend across VR7 (Fig.5A).

5. Discussion

5.1. Submarine volcanism

Detailed bathymetric mapping makes it possible to immediately identify two types of morphologies rising over an abyssal plain at depth locally exceeding 3,500 m (Fig.1B, F): (1) central volcanoes forming islands and their submarine bedrock, and (2) elongated volcanic ridges, more or less prominent above the abyssal plain, interconnecting, or not, these islands (Fig.1 and Table1). This is a major morphological character of the Comoros archipelago.

Overall morphology of the submarine volcanic islands' flanks

511 As for many other volcanic islands (e.g. Gee et al., 2001; Mitchell et al. 2002, 2003;
512 Geist et al. 2006; Masson et al. 2002; 2008; Chiocci et al 2013), the submarine flanks
513 of the Comorian Islands show constructional volcanic areas and slopes that have
514 undergone erosive-depositional processes. Volcanic constructional flanks (Mitchell et
515 al., 2002) are recognized from their rough and uneven morphology, due to the
516 presence of numerous volcanic cones, eruptive fissures and lava flows. They are
517 interpreted as directly built by volcanic eruptions, even if they may have undergone
518 later erosion and sedimentation. The presence of numerous volcanic cones and
519 alignments of volcanic cones characterizes the constructional submarine flanks of the
520 Comoros Islands. Data resolution does not allow clear identification of lava flows, even
521 if lobate outlines are sometimes identifiable. For Grande Comore, Anjouan and Mohéli,
522 average slope gradients of the constructional flanks are almost steady (about 8° to 10°)
523 or slightly decreasing downslope (lines 3 to 10 on Fig.10A). In comparison to the other
524 Comorian Islands, Mayotte's submarine slopes are gentler (~ 5° - line 11 on Fig.10A)
525 and smoother, reflecting a significant spreading of the formations building the
526 submarine flanks of this island and a higher sediment cover. Sediments are largely
527 covering Mayotte's submarine flanks, while few volcanic cones are identifiable, except
528 for the northwest (VR5) and the east (VR6) of the island (Fig.5A).

529 Compared to constructional ones, flanks affected by landslides show smoother
530 surfaces and have slope profiles showing a clear gradual decrease in slope gradient,
531 passing from steep upper slopes (>40°) to downslope moderate (3-10°) gradients (Fig.
532 10B). For some of them, the profile changes in the mid-slope from concave to locally
533 slightly convex, likely determined by deposit accumulation (lines 1, 3, 5 on Fig.10B).
534 Landslide scars at the insular shelf edges and coastlines can be frequently identified
535 upslope these flanks. The general morphology of the deposit accumulations,

sometimes defining a fan-shaped bulge with blocky and hummocky surface morphology, allows us to interpret these deposits as debris avalanche deposits. Such flank morphologies, the general shape of the deposits and the occurrence of upslope landslides scars, allow to infer that these morphologies are likely related to large-scale failure events. They are similar to what has been described for many other volcanic islands (e.g., Canary Islands, Ablay and Hürlimann, 2000; Masson et al., 2002; Acosta et al., 2003; Mitchell et al., 2002; Hunt et al., 2014; Cape Verde, Masson et al., 2008; Aeolian Islands, Romagnoli et al., 2009, 2013; Hawaiian Islands, Moore et al., 1989; Moore et al., 1994; Morgan et al. 2003; La Reunion Island, Oehler et al., 2008; Le Friant et al., 2011).

Volcanic rift zones

The existence of volcanic rift zones characterizes the subaerial part of the Comorian shield volcanoes (Bachèlery et al., 2016; Famin et al., 2020). Volcanic rift zones are preferential pathways that transport magma from a shallow magma reservoir to the flank of the volcano. They are caused by internal and gravitational stresses (e.g. Dieterich, 1988; Tilling and Dvorak, 1993). In Grande Comore, the volcanic rift zones are well defined by alignments of cinder and spatter cones along eruptive fissures. They form a typical ridge-like topography (Bachèlery et al., 2016). The shape of Anjouan is clearly reminiscent of the youngest Canary Islands El Hierro, Tenerife and La Palma, with wide coastal embayments and a three-armed geometry corresponding to volcanic rift zones. Such an association, with triple ‘Mercedes Star’ rift zones and giant lateral collapses affecting the flanks of these rift zones, reveals a growth of the volcanic edifice controlled by active volcanism (Carracedo, 1994, 1996).

560 With the exception of the SE rift zone of Karthala (Fig. 2), which extends to a depth of
561 about 1,000 m, with an average slope of ~4° before connecting with VR3 (line 1 on
562 Fig.10A), and possibly the rift zones of Anjouan, the submarine slopes do not show any
563 significant offshore extension of the volcanic rift zones recognized on land. This is for
564 example the case for the volcanic rift zones north of the Karthala and Grille massifs
565 (Fig. 2A).

566 In the Comoros Islands, submarine flanks built by repeated intrusive/eruptive activity
567 (constructional flanks) form areas, extending up to ~ 20 km from the coast, whose
568 morphologies range from *short linear ridges*, as the SE rift zone of Karthala volcano
569 and the S rift zone of Anjouan, to a broader *"fan-like"* geometry, as for the
570 constructional flanks of Mohéli and the northern submarine flanks of La Grille Massif
571 and Anjouan. The Comoros Islands do not have well-developed rift zones as those
572 around Hawaiian Islands, spreading up to 50 km from the coast. Actually, they have
573 similarities with those observed in La Réunion Island (Lénat et al., 2012), the
574 Galapagos Islands (Geist et al. 2006) or the Canary Islands (Gee et al, 2001; Mitchell
575 et al, 2002; Acosta et al., 2003). Such morphologies suppose a reduced capacity for
576 magma to laterally intrude into the rift zones, from underlying magma chambers.
577 Acosta et al. (2003) have already discussed this difference in morphology for the
578 Canary Islands. The main similarities between Comoros and Canary archipelagoes lie
579 in the chemical composition of the magmas (both alkaline, versus more tholeiitic
580 magmas for the Hawaiian shields), a low magma production rate, a more complex
581 history of volcano building, a slow absolute plate motion, and a lesser depth of the sea
582 floor around the islands and consequently, a lesser elevation of the islands above it.
583 This influences the gravitational stress field on volcanic edifices and the ability of
584 magma to propagate into rift zones.

585

586 **Submarine volcanic ridges**

587 Eight major volcanic ridges have been identified from the bathymetric data (VR1 to 8).
588 They are elongated, steep-sided reliefs, with numerous volcanic cones and alignments
589 of volcanic cones. Their volcanic origin can be deduced from the acoustic texture and
590 the morpho-bathymetric analyses revealing their uneven morphology and, for some of
591 them, the youthfulness of remarkably preserved reliefs. The aligned distribution of the
592 volcanic cones and orientation of the volcanic ridges suggest that they are built along
593 lithospheric fault system (Muffler et al., 2011). Three of the volcanic ridges are located
594 between the main islands of the archipelago (between Grande Comore and Mohéli -
595 VR3, between Mohéli and Anjouan - VR4, and between Anjouan and Mayotte - VR5)
596 (Fig.1C, D, E). Furthermore, VR2 connects Grande Comore to the old volcanic edifice
597 of Vailheu Bank (Fig.1, 2 and line 2 on Fig.10A). This indicates strong interaction
598 between active tectonic and volcanic processes (Duffield et al., 1980; Bacon, 1982;
599 Connor and Conway, 2000; Valentine and Krogh, 2006; Gaffney et al., 2007).

600 The average depth of these volcanic ridges increases from Grande Comore to Mayotte
601 (Fig. 1F). Between Anjouan and Mayotte, the ridge VR5 is less discernible but we
602 suggest its existence, based on a clearly positive morphology (see profile ‘d-e’ in Fig.4)
603 and the higher density of cones. The fact that this ridge is less visible could be
604 explained by an older age of volcanic activity and a partial blanketing by sedimentary
605 cover. The volcanic ridge VR6 (site of the ongoing eruption – Fig. 5) spreads from the
606 eastern flank of Mayotte. Cones, eruptive fissure ridges, lava flows and plateaus,
607 mounds, and inflated lava flow have been recognized along and near this volcanic
608 ridge (Paquet et al., 2019).

609 Without collected samples, we can only postulate that the volcanic activity on the
610 volcanic ridges of the Comoros archipelago is probably mainly related to mafic
611 magmatism along active lithospheric fissure systems, as indicated by the prevalence of
612 pointy morphology of the volcanic cones and their frequent alignment, as observed for
613 other oceanic volcanic islands (e.g. Casalbore et al., 2015; Clague et al., 2019).
614 However, more evolved compositions (intermediate and silicic magmas) may have
615 been locally responsible of eruptions, as evidenced by the variability of composition of
616 the magmas dredged on the ridge east of Mayotte (VR6), and the evolved
617 compositions of the magmas feeding the 2018 – 2020 eruption off Mayotte (Bachèlery
618 et al. 2019; Berthod et al. submitted). These volcanic ridges can be considered as
619 'monogenetic volcanic fields', resulting from multiple episodic eruptions building
620 monogenetic volcanoes (see Smith and Németh, 2017, Németh and Kereszturi, 2015).
621 If so, this implies the genesis of magma batches below the volcanic ridges in discrete
622 fusion events with a defined chemical composition (Smith and Németh, 2017). Their
623 distribution provides evidence of the existence of lithospheric fractures allowing
624 episodic access for deep magmas. However, we are aware that high-resolution studies
625 of the Comorian submarine volcanic ridges need to be carried out in order to verify their
626 origin.

627

628 **Volcanic cones and mounds**

629 A large number of volcanic cones crop out offshore the Comoros Islands. They are
630 found at all depths, even if about 70% of them are located at more than 2,000 m bsl.
631 Volcanic cones are mostly present on the submarine flanks of the islands and on the

volcanic ridges, but also isolated on the abyssal plain, sometimes at more than 70 km from the nearest island (Fig.6C, F).

Some 1,650 volcanic cones have been measured on the surveyed area. The morphological parameters (regular shape, conical to elliptical, size and aspect ratio) are those classically encountered for submarine cones around volcanic islands or ridges (Clague et al., 2000; Romero Ruiz et al., 2000, Mitchell et al., 2012; Casalbore et al., 2015; Romagnoli et al., 2020). Some morphometric parameters of the volcanic cones encountered in the Comoros archipelago are shown in Fig. 11. These values are similar to those obtained for the submarine pointed cones of the Azores (Stretch et al., 2006; Mitchell et al., 2012; Casalbore et al., 2015; Weiß et al 2015), or Linosa, Sicily Channel (Romagnoli et al., 2020) and a bit different from those in Canary (Mitchell et al., 2002; Romero Ruiz et al., 2000) and Hawaii (Clague et al., 2000; Wanless et al., 2006) with values around 0.08 (Fig.11). The highest volcanic cones (over 300 m in height) have a slightly higher than average aspect ratio (0.21 vs. 0.15), reflecting smaller diameter with respect to the cone height. This suggests that they develop preferentially upwards rather than outwards. As shown by the 'Cône Elianne', a 700 m high volcanic cone on the southern flank of Piton de la Fournaise volcano, La Réunion (Saint-Ange et al., 2013; Michon et al., 2016) or by the more than two-years-long ongoing eruption located on the volcanic ridge (VR6) off the eastern coast of Mayotte (Feuillet et al., 2019), the significant size of the Comorian submarine pointed cones (120 m in average, and up to 820 m high for the Mayotte ongoing eruption) may be related to a long duration of eruption and the high initial volatile content of the alkalic magmas emitted along the archipelago. It is difficult to infer eruptive regimes based only on the analysis of bathymetric data. Many parameters are involved, such as water depth, magma discharge rate and composition, including volatile content. The eruption

657 of chemically homogeneous, undegassed, volatile-rich, magma may favor formation of
658 pointed cones (Clague et al., 2000; Wanless et al., 2006).

659 Around the Comoros Islands, rare flat-topped cones (Fig.6F, 7D) have been observed,
660 always at great depths. They are considered as the result of long-lived steady effusive
661 eruption of magma of low viscosity and volatile content, at low to moderate effusion
662 rate, on low slopes (Clague et al., 2000; Wanless et al., 2006).

663 Several mounds have been recognized throughout the Comoros archipelago, on the
664 abyssal plain or next to volcanic ridges (Fig.12), in areas where a sedimentary cover
665 allows their injection: SW of Grande Comore (Fig.2A, C) and NE of Anjouan (Fig.4A,
666 Fig.6C). Compared to volcanic cones, their aspect ratio (H/W) is very low (<0.04)
667 (Fig.7B, 11). Mounds are considered as surface expressions of flat magmatic intrusive
668 bodies (sill-type intrusions) emplaced at shallow structural level and related to
669 hydrothermal–volcanic activity (Medialdea et al., 2017; Sanchez-Guillamón et al.,
670 2018). Magma injection causes differential uplifting, forced folding and faulting of the
671 overlying sedimentary layers, and can induce the transport of hot fluids to the surface.
672 According to the morphostructural classification of Sanchez-Guillamón et al. (2018)
673 based on the Canary Basin, the Comorian mound morphologies are similar to the
674 subcircular mounds corresponding to the morphostructural type 2 (group A), in good
675 agreement with a sill-like intrusion into the sedimentary cover (Sanchez-Guillamón et
676 al., 2018). We identify small-scale faulting along the summit and the flanks of the
677 mounds (Fig.8A, B), which can be interpreted as vertical fracture pipes and hence fluid
678 migration pathways, and forced folds near the base that may result from the elevation
679 generated by the intrusive bodies (Sanchez-Guillamón et al., 2018). However, lower-
680 resolution seismic profiles or multichannel profiles are needed to better characterize
681 the magmatic activity and to image the internal structure of the mounds, to confirm the

682 presence of sill intrusions and the location of hydrothermal vent complexes, as well as
683 their age.
684
685 **5.2. Erosive-depositional processes**
686 Unfortunately, no information is available on the age of the mass-wasting events, but
687 the presence of bedforms, scars and debris avalanche deposits indicate very active
688 mass-wasting processes on the submarine portions of the Comorian islands.
689
690 **Large-scale and small-scale instabilities**
691 Large-scale failure events have been identified from flank morphology, the existence of
692 hummocky terrains interpreted as debris avalanche deposits and the occurrence of
693 upslope horseshoe-shaped scars (see *Overall morphology of the submarine volcanic*
694 *islands' flanks*). Large-scale flank instability events may radically change the
695 topographic profile of the affected area and this change remains perceptible even if
696 subsequent events occur (Masson et al., 2002). Landslide scars at the insular shelf
697 edge are common features observed along the submarine flanks of insular volcanoes
698 (Casalbore et al., 2014, Chiocci and Casalbore, 2017; Ricchi et al., 2020).
699 Well-defined amphitheater-shaped structures that could correspond to landslide's scars
700 are easily identified southwest of the Karthala Massif, south of Mohéli, north and south
701 of Anjouan and southeast of Mayotte (respectively Fig.2, 3, 4 and 5). Fan-shaped
702 bulges and hummocky terrains, interpreted as debris avalanche deposits, cover the
703 submarine flanks downslope the landslide scars (Fig.6D, G). Slope gradient maps
704 allow to better evidence units suggesting that the submarine bulges have formed by the

705 emplacement of multiple mass-wasting deposits (Fig.7A). We assume that the
706 hummocky surface morphology of the debris avalanche deposits is shaped by a large
707 number of blocks. However, the resolution of the bathymetry does not allow to finely
708 characterize these hummocky surfaces. As previously mentioned, we cannot surely
709 identify megablocks, and it would be unreasonable to try to distinguish them from
710 volcanic cones that could have been built after the debris avalanche deposition. Data
711 with a higher resolution need to be acquired to better characterize these deposits and
712 to verify the existence of volcanic cones built *a posteriori*. It is also crucial to determine
713 the age of the deposits and their exact meaning in the evolution of the islands.

714 Southeast of Karthala volcano, the amphitheater-shaped structure is small (Fig. 2A),
715 irrelevant with respect to the extension of the debris avalanche deposits observed on
716 the submarine flank of this volcano. This implies that the volcanic activity in this area
717 lasted long enough after the debris avalanche deposit, to build a convex coastline and
718 cover most of the landslide scar associated with these deposits. The overall
719 morphology is quite different for the flank landslides identified in Mohéli, Anjouan and
720 Mayotte, for which landslide scars are clearly identifiable, implying reduced volcanic
721 activity after the collapse. In Mayotte, a large amphitheater-like scar is visible cutting
722 across the southeastern edge of the insular shelf (affecting T1May). However, we
723 cannot identify associated debris avalanche deposits. Except for the submarine
724 volcanic ridge at the east of the island (VR 6), the submarine flanks of Mayotte have
725 smooth and gentle slopes with many small slope failures and channels. The spreading
726 of volcaniclastic products appears to be wider than for the other islands of the
727 archipelago (Fig.10A), probably related to the greater age of Mayotte volcanism, and
728 thus the prevalence of gravitational processes of erosion/deposition over a longer
729 period of time.

730 Collapsed debris, related to small-scale mass-wasting events, are observed on the
731 outer edge of the insular shelves of Mohéli (Fig.3B, 6A) and Mayotte (Fig.5C), similarly
732 to that observed in the Aeolian Islands of Lipari, Stromboli and Vulcano (Casalbore et
733 al., 2011; Romagnoli et al., 2013; Casalbore et al., 2016). Most recent landslides are
734 identified by the presence of collapsed debris deposits on the terraces T2May and
735 T3May (Fig.5A, C, D). Some of the debris deposits are large in size reaching 0.5 km^2
736 and can be associated with landslide scars affecting the insular shelf edge, the terraces
737 and the upper slopes.
738

739 **Gravity flows processes and associate submarine landforms**

740 Submarine channel systems are developed diversely depending on the islands,
741 indicating evolutionary differences. Some islands are surrounded by well-developed
742 submarine canyon-channel systems (i.e. Mayotte), while others are characterized by
743 younger and little developed channel systems (i.e Grande Comore) (Fig.12). We
744 consider that the younger islands tend to have a high volcanic activity and a poorly
745 developed hydrographic system both in the mainland and the submarine section, as it
746 is the case for Grande Comore . On the contrary, numerous channels drain oldest
747 volcanic islands' submarine flanks, while a very low density of cones is present, such
748 as for Mayotte.

749 The development of channels may be related to the overall shape of the volcanic
750 edifice. The submarine channels around the islands mainly have a straight morphology
751 resulting from the steepness of the uppermost and mid-slopes of the islands (Clark et
752 al., 1992). However, as the slopes decrease (around 20°), gullies and channels
753 converge and gradationally merge downslope into a single channel (Mo1 and Mo3 in

754 Mohéli, Anj2 and Anj7 in Anjouan, and the majority of Mayotte's channels), while in
755 some cases, channels bifurcate and split into multiple channels (GC3 and GC4 in
756 Grande Comore). Around Mayotte, the extensive incision of gullies and channels in the
757 submarine flanks and their sinusoidal shape confirm the maturity of its channelized
758 system. The channels' heads mostly affect the outer edge of the insular shelf/marine
759 terraces (Fig.5C) and their formation likely started at the time these terraces were
760 emerged (as proposed by Audru et al., 2006) during low-stands of the relative sea
761 level.

762 On the upper steep slopes of the volcanic edifices (> 20°), no bedforms are formed but
763 gullies or/and channels incise the flanks of the islands. The sediment-laden flows erode
764 the seafloor impeding the formation of small-scale bedforms (Schlager and Camber,
765 1986; Micallef and Mountjoy, 2011; Clare et al., 2018). In higher water depths ranging
766 from 1,400 m to 3,500 m and when flanks gradients decrease (<20°), large-scale
767 bedforms occur throughout the archipelago, with a range of wavelengths and wave
768 heights being respectively, 1 to 2,7 km and 15 to 80 m (Fig.9). Where the channelized
769 system is well developed, large-scale bedforms, with an average wavelength of 1.5 km
770 are sometimes present between the channels, as it is the case for Mohéli and Mayotte
771 (Fig.3, 5). Bedforms are also present inside the channels of Mohéli and Mayotte, but
772 are smaller in size than those in the interfluve (Fig.9). According to Cartigny et al.
773 (2011), bedforms in the interfluves correspond to potential overspilling locations,
774 assuming that bedforms form perpendicular to the flows. Gravity flows or unconfined
775 turbidity currents might be at the origin of the bedforms, and the frequent change in the
776 gradient slope of the bedforms as seen in Fig.9, the result of the changes in flow
777 thickness, velocity and specific discharge (e.g. Wynn et al., 2002; Cartigny et al., 2011;
778 Postma & Cartigny, 2014). The development of volcaniclastic turbidite systems is

779 associated with these large-scale bedforms, result of unconfined gravity flows mainly
780 supplied from riverine input (Mazuel et al., 2016), which correspond to the Comoros
781 case. The same morphologies have been reported in Stromboli and Panarea Islands
782 (Sicily) and La Réunion Island (Mazuel et al., 2016; Casalbore et al., 2020). Also, the
783 southern flank of Mohéli clearly reminds the northern flank of Porto Santo of the
784 Madeira archipelago (Casalbore et al., 2020), where bedforms located in the flanks of
785 the islands are associated to the arcuate headwall scars, resulting from gravity flows
786 originated by seafloor displacements.

787

788 **5.3. Relative chronology of the volcanism**

789 The chronology of the volcanism along the Comoros archipelago is still an open
790 question. Mayotte's morphology, with its wide shelf and well-developed fringing reef,
791 contrasts with that of the little eroded and active shield volcanoes in Grande Comore.
792 This suggests a rejuvenation of volcanism from east to west. Nevertheless, the ongoing
793 eruption 50 km east of Mayotte is disrupting this pattern (Fig.12). Some considerations
794 and a relative chronology of the volcanism can be deduced from geomorphological
795 features, erosion stages, the presence or absence of a developed insular shelf and
796 terraces, the overall shape and gradient of slopes, the more or less developed
797 channelized systems and the abundance of volcanic cones (Fig.12).

798 Grande Comore and Anjouan are high altitude volcanic islands with only very narrow
799 shelves and no submarine terraces visible today. Pristine volcanic morphologies, with
800 numerous volcanic cones, eruptive fissures and lava flows, are clearly identifiable on
801 Grande Comore (Bachèlery et al., 2016), while ash cones are well preserved and little
802 affected by erosion on Anjouan (Nougier et al, 1986; Famin et al., 2020), enabling

803 volcanic rift zones to be identified for these two islands (Fig.12). In contrast, Mohéli and
804 Mayotte are lower islands characterized by a well-developed insular shelf, as well as
805 ancient terraces located between 450 and 600 m bsl for Mohéli (T2Moh and T3Moh)
806 and between 450 and 830 m bsl for Mayotte (T2May and T3May).

807 Terraces are considered as paleo-sea level markers (Casalbore et al., 2017; Ricchi et
808 al., 2018). We have no information about the nature and age of the Mohéli terraces.
809 Concerning Mayotte, the channels and karst systems on the insular shelf would have
810 been formed at the end of the last glacial maximum (20 to 18 kyr), when the lagoon
811 and the reef emerged (Dullo et al., 1998; Audru et al., 2006; Montaggioni and Martin-
812 Garin, 2020). For Audru et al. (2006), the two terraces of Mayotte, now underwater,
813 would have also formed in the subaerial domain, as shown by the presence of erosion
814 channels on their surface. They propose that they were formed during the Pliocene (2.6
815 Ma and 3.9 Ma for T2May and T3May, respectively), based on their average depth,
816 and considering a steady subsidence rate of 0.19 mm/year. Even considering a higher
817 subsidence rate (0.25 mm/year, Camoin et al., 1997; Montaggioni and Martin-Garin,
818 2020), this indicates that, on Mayotte, erosion dominates over volcanism during the last
819 million years. Wider shelves, like those of Mohéli and Mayotte, are commonly
820 associated with older volcanic centers (Romagnoli et al., 2018). The strong
821 indentations of the coastline or insular edge also confirm the advanced stage of these
822 islands. Although little is known about the terraces of Mayotte and Mohéli, the common
823 features regarding their insular shelves and terraces (depth, size) argue in favor of a
824 similar origin and age, and seem to indicate a common geological history of these two
825 islands. The presence of terraces at great depths provides evidence of subsidence that
826 has affected the islands of Mayotte and Mohéli, but without independent age control, it

827 is not possible to decipher the relative effects of sea level fluctuations and active
828 subsidence of the volcanic substratum.

829 The Grande Comore volcanoes show a typical shield volcano morphology little
830 modified by erosion, similar to the volcanoes of Big Island – Hawaii. Many volcanic
831 cones are visible on the submarine slopes of Grande Comore, in accordance with the
832 young age of this edifice and its frequently active volcanism. The morphology of
833 Anjouan also shows strong similarities with that of volcanic islands with recent volcanic
834 activity, by its modeled embayments and its triple-armed geometry rift zones, which
835 indicate, according to Macdonald (1972), active rift zones (see 5.1. Rift zones). Primary
836 volcanic morphologies (volcanic cones, alignments of volcanic cones) are also
837 particularly well preserved on the submarine flanks of the islands of Grande Comore
838 and Anjouan, compared to Mohéli and Mayotte. Volcanic cones appear less numerous
839 and less easily identifiable on the smoother submarine flanks of these islands. In
840 addition, eroded volcanic bedrock, submarine flanks with multiple slope breaks and
841 gentle slopes obscured by a significant sedimentation and widespread volcaniclastic
842 deposits, surround Mayotte. Finally, the channelized system around Anjouan is less
843 developed compared to Mohéli, while around Mayotte the channels are prevalent on
844 the whole submarine flanks.

845 The morphological considerations listed above indicate that, if Mayotte is indeed the
846 oldest of the islands of the Comorian archipelago, Mohéli is significantly older than
847 Anjouan. Anjouan could therefore be the second youngest island in the archipelago
848 after Grande Comore. The available geochronological data seem to suggest that
849 Mohéli would be younger than Anjouan. But the paucity of geochronological data, and
850 the fact that all dated rocks belong to the subaerial domain, explain this discrepancy

851 with our conclusions. Thus, the progression of ages along the Comorian archipelago
852 must be reconsidered.

853 Michon et al. (2016) propose that volcanic activity in Mohéli and Anjouan began 7 to 10
854 Ma ago, about 10 Ma later than in Mayotte. As the oldest islands appear to be Mayotte
855 and Mohéli, we can assume that volcanism migrated northward from these volcanic
856 centers, to extend to Anjouan and later to Grande Comore. The formation of the
857 volcanic ridges of the Jumelles on the seafloor in the east of Mayotte, seems to be
858 recent, as shown by the morphological freshness of these ridges, the high density of
859 volcanic cones, and the paucity of sediment coverage (Fig.8C). In the same way, the
860 current eruption in the east of Mayotte Island (Feuillet et al., 2019) is a magnificent
861 illustration of the possibilities of resuming activity after several millennia of rest. This
862 clearly demonstrates that, throughout the archipelago, volcanism can resume at any
863 time.

864

865 **5.4. Structural control on volcanism**

866 One of the outstanding features of volcanism in the Comoros Archipelago is the
867 existence of submarine volcanic ridges interconnecting the main islands (Fig.1 and 12).
868 This unique pattern, with a close association of main central volcanoes at different
869 stages of evolution, like those of Grande Comore, Mohéli, Anjouan and Mayotte, and
870 volcanic ridges composed of the juxtaposition of many monogenetic volcanic edifices,
871 highlights a strong link between regional tectonics and magmatism. Linear volcanic
872 ridges can be considered as the result of magma emplacement into a pre-existing
873 damaged lithosphere (Neves et al., 2013). They can be seen as the surface expression
874 of a monogenetic magmatism controlled by lithospheric extension along the ridge axis,

875 which, for the Comoros archipelago, could correspond to the diffuse plate boundary
876 between the Somali Plate and the Lwandle Plate, as proposed by Famin et al. (2020).
877 Indeed, in areas close to volcanic ridges, such as west of Grande Comore or east of
878 Mohéli, bedforms probably emanating from compressional zones occur, due to a
879 morphological expression of thrust.

880 Two main sets of tectonic orientations (Fig.12) are highlighted by the distribution of
881 volcanic ridges, but also by the directions of volcanic rift zones and small-scale
882 elongated volcanic features such as alignments of cones and faults (Fig.6C, 6F). The
883 first group corresponds to structures ranging from N120° to N160°, with the volcanic
884 ridges VR2, VR5, VR6, VR7 and VR8, the rift zones SE of Karthala volcano and SE of
885 Anjouan, and alignments of cones (e.g. NE of Anjouan and N of Grande Comore). A
886 second group is composed of globally oriented WSW-ENE ridges, with the volcanic
887 ridges VR1 and VR3, and alignments of cones (e.g. north of VR8 and across VR7).
888 These orientations are coherent with regional extensional and trans-tensional fault
889 systems as reported by Deville et al. (2018) for the southern part of the Mozambique
890 Channel, or normal fault escarpments observed along the Sakalaves Seamounts by
891 Courgeon et al. (2018). Available focal mechanisms near the Comoros Islands (Fig.12)
892 indicate normal faulting and strike slip, with an orientation compatible to a NE-SW
893 tensional axis (Lemoine et al. 2020). Thus, the revelation of volcanic ridges along the
894 seafloor of the Comoros archipelago is consistent with the interpretation of the
895 Comoros archipelago as a dextral shear zone potentially being the northern boundary
896 of the Lwandle plate, as proposed by Famin et al., 2020. As for Canary Islands (Geyer
897 and Martí, 2010), the origin and evolution of the volcanic islands of the Comorian
898 archipelago are strongly controlled by regional tectonic structure. In such a context, the
899 main volcanic islands constituting the Comoros archipelago have grown over the main

900 loci of genesis and magma transfer, whereas a more diffuse volcanism occur along the
901 volcanic ridges.
902
903 **6. Conclusions**

904 The morpho-bathymetric analysis of the Comoros archipelago allowed us to
905 discover the shape and geomorphology of each island's submarine flanks, from their
906 insular shelf to the abyssal plain. The Comorian volcanic edifices include both active
907 volcanic edifices and volcanic islands with well-developed carbonated insular shelves
908 (up to 10 km wide from the coast to the insular shelf edge) and terraces located at
909 depth of more than 400 m. Despite the geographical location of the islands,
910 geomorphological analyses (e.g. erosion stages, presence or absence of a developed
911 insular shelf and terraces, overall shape and gradient of slopes of the submarine
912 flanks, more or less developed channelized systems) clearly show that Mayotte and
913 Mohéli Islands are on top older edifices compared to Anjouan and Grande Comore. We
914 propose a new relative chronology concerning the Comorian volcanism, the youngest
915 to the oldest islands being respectively, Grande Comore, Anjouan, Mohéli and Mayotte.
916 Large-scale instabilities and debris avalanche deposits, gravity flows processes and
917 large-scale bedforms, channelized system maturity and density of volcanic cones and
918 mounds have also been described.

919 One of the major volcanological and structural features of Comorian volcanism is
920 the close coexistence of central volcanoes forming islands, with elongated volcanic
921 ridges interconnecting, or not, these islands. The existence of submarine volcanic
922 ridges interconnecting the central volcanoes highlights the close link between regional
923 tectonics and magmatism. The magmatic feeding of the Comoros archipelago seem to

occur with, on the one hand, a strong magmatic supply focused under one or several main volcanoes at different stages of evolution, and on the other hand, a magmatism located along elongated volcanic ridges, controlled by lithospheric extension and composed of monogenetic edifices. The orientation of the volcanic ridges coincides to the regional faulted structures interpreted as the seaward prolongation of the East African Rift and those of Madagascar. The Comorian volcanism seem to be strongly connected with the regional lithospheric fractures, induced by the Somalian/Lwandle plates boundary and/or the Karoo rifting episodes. The genesis of the Comoros archipelago is most probably linked to lithospheric deformations, rather than the unique result of a deep mantle plume motion.

Acknowledgments

The authors would like to thank the technical and scientific shipboard parties of the R/V *Marion Dufresne* (BATHYMAY cruise), the Shom (French Hydrographic Office) and the BRGM (French Geological Survey) for the high resolution data acquired with multibeam echosounders, but also for Lidar surveys conducted under the Litto3D® program by the Shom. An additional thank to the technical and scientific shipboard parties of the BHO *Beautemps-Beaupré* for the acquisition of high resolution seismic profiles (CHIRP). Finally, we would like to thank the five reviewers, including Daniele Casalbore, Laurent Michon, Claudia Romagnoli and Luis Somoza, without their expertise and constructive comments, this paper could not have taken its complete and structured form. This is a LabEx Clervolc contribution n° XXXX.

945 **References**

946 Ablay, G. J., and M. Hürlimann., 2000. Evolution of the north flank of Tenerife by
947 recurrent giant landslides, J. Volcanol. Geotherm. Res., 103, 135–159,
948 doi:10.1016/S0377-0273(00)00220-1.

949 Acosta, J., Uchupi, E., Smith, D., Muñoz, A., Herranz, P., Palomo, C., Llanes, P.,
950 Ballesteros, M., ZEE Working Group. 2003. Comparison of volcanic rifts on La
951 Palma and El Hierro, Canary Islands and the Island of Hawaii. Mar. Geophys. Res.
952 24, 59–90. DOI 10.1007/s11001-004-1162-6.

953 Audru, J.-C., Guennoc, P., Thinon, I., Abellard, O., 2006. Bathymay : la structure sous-
954 marine de Mayotte révélée par l'imagerie multifaisceaux. Comptes Rendus
955 Geoscience 338, 1240–1249. DOI: 10.1016/j.crte.2006.07.010

956 Bachèlery, P., Coudray, J., 1993. Carte volcano-tectonique (1/50000e) de la Grande
957 Comore et notice explicative, In: Coopération MFdl (ed) Carte Géologique des
958 Comores. Ministère Français de la Coopération.

959 Bachèlery, P., Ben Ali, D., Desgrolard, F., Toutain, J.P., Coudray, J., Cheminee, J.L.,
960 Delmond, J.C., Klein, J.L., 1995. L'éruption phréatique du Karthala (Grande
961 Comore) en juillet 1991. Comptes Rendus Académie Sciences Paris 320 (II–a):691–
962 698.

963 Bachèlery, P., Villeneuve, N., 2013. Hotspots and large igneous provinces. In: Shroder,
964 J. (Editor in Chief), Owen, L.A. (Ed.), Treatise on Geomorphology. Academic Press,
965 San Diego, CA, vol.5, Tectonic Geomorphology, pp. 193–233.

966 Bachèlery, P., Morin, J., Villeneuve, N., Soulé, H., Nassor, H., Radadi Ali, H., 2016.
967 Structure and eruptive history of Karthala volcano. In Active Volcanoes of the
968 Southwest Indian Ocean, edited by Patrick Bachèlery, Jean-François Lénat, Andrea

969 Di Muro, and Laurent Michon, 333–44. Berlin, Heidelberg: Springer Berlin
970 Heidelberg. https://doi.org/10.1007/978-3-642-31395-0_22.
971 Bachèlery, P., Berthod, C., Di Muro, A., Gurioli, L., Besson, P., Caron, B., ... & Deplus,
972 C., 2019. Petrological and Geochemical Characterization of the Lava from the 2018-
973 2019 Mayotte Eruption: First Results. AGU, Fall Meeting San Francisco, V52D-06.
974 Bacon, C.R., 1982, Time-predictqble bimodal volcanism in the Coso Range, California:
975 Geology, v.10, p.65-69
976 Berthod, C., Médard, E., Bachèlery, P., Gurioli, L., Di Muro, A., Peltier, A., Komorowski,
977 J-C., Benbakkar, M., Devidal, J-L., Langlade, J., Besson, P., Boudon, G., Rose-
978 Koga, E., Deplus, C., Le Friant, A., Bickert, M., Nowak, S., Thinon, I., Burckel, P.,
979 Hidalgo, S., Kaliwoda, M., Jorry, S., Fouquet, Y., Feuillet, N. The 2018-ongoing
980 Mayotte submarine eruption: magma migration imaged by petrological monitoring.
981 Earth Planet. Sci. Lett., submitted.
982 Binard, N., Hekinian, R., Stoffers, P., 1992. Morphostructural study and type of
983 volcanism of submarine volcanoes over the Pitcairn hot spot in the South Pacific,
984 Tectonophysics, 206 (1992), pp. 245-264, https://doi.org/10.1016/0040-
985 1951(92)90379-K.
986 Biscara, L., Maspataud, A., Schmitt, T., 2016. Coastal risk assessment: Generation of
987 bathymetric digital elevation models along French coasts. Hydro International,
988 September 2016, 26-29. http://www.hydro-international.com/content/article/coastal-
989 risk-assessment.
990 Bourhane, A., Comte, J.-C., Join, J.-L., Ibrahim, K., 2016. Groundwater Prospection in
991 Grande Comore Island—Joint Contribution of Geophysical Methods,
992 Hydrogeological Time-Series Analysis and Groundwater Modelling, in: Bachèlery,
993 P., Lenat, J.-F., Di Muro, A., Michon, L. (Eds.), Active Volcanoes of the Southwest

994 Indian Ocean. Springer Berlin Heidelberg, Berlin, Heidelberg, pp. 385–401.
995 https://doi.org/10.1007/978-3-642-31395-0_24.
996 Camoin, G.F., Davies, P.J. (Eds.), 1998. Reefs and carbonate platforms in the Pacific
997 and Indian oceans, Special publication number 25 of the International Association of
998 Sedimentologists. Blackwell Science, Oxford; Malden, MA, USA.
999 Camoin, G.F., Montaggioni L.F., Braithwaite C.J.R., 2004. Late glacial to post glacial sea
1000 levels in the western Indian ocean. Marine geology, 206, 119-146.
1001 Carracedo, J. C., 1994. The Canary Islands: an example of structural control on the
1002 growth of large oceanic-island volcanoes, Journal of Volcanology and Geothermal
1003 Research, 60 (3-4), 225-241.
1004 Carracedo, J.C. 1996. Morphological and structural evolution of the western Canary
1005 Islands: hotspot-induced three-armed rifts or regional tectonic trends?, Journal of
1006 Volcanology and Geothermal Research, vol. 72, pp. 151-162
1007 Cartigny, M.J.B, Postma, G., van den Berg, J.H., Mastbergen, D.R. 2011. A comparative
1008 study of sediment waves and cyclic steps based on geometries, internal structures
1009 and numerical modeling. Marine Geology, Vol. 280 (2011), pp. 40-56.
1010 https://doi.org/10.1016/j.margeo.2010.11.006
1011 Casalbore, D., Romagnoli, C., Bosman, A., Chiocci, F.L. 2011. Potential tsunamigenic
1012 landslides at Stromboli Volcano (Italy): Insight from marine DEM analysis,
1013 Geomorphology 126 (2011) 42-50.
1014 Casalbore, D., Romagnoli, C., Pimentel, A., Quartau, R., Casas, D., Ercilla, G., Hipólito,
1015 A., Sposato, A., Chiocci, F.L., 2015. Volcanic, tectonic and mass-wasting processes
1016 offshore Terceira Island (Azores) revealed by high-resolution seafloor mapping, Bull
1017 Volcanol (2015) 77:24, DOI 10.1007/s00445-015-0905-3.

1018 Casalbore, D., Bosman, A., Romagnoli, C., Di Filippo, M., Chiocci, F.L. 2016.
1019 Morphology of Lipari offshore (Southern Tyrrhenian Sea), Journal of Maps, 12:1, 77-
1020 86, DOI: 10.1080/17445647.2014.980858
1021 Casalbore, D. 2018. Volcanic islands and seamounts. In Submarine Geomorphology, pp.
1022 333-347. Springer, Cham.
1023 Casalbore, D., Clare, M.A., Pope, E.L., Quartau, R., Bosman, A., Chiocci, F.L.,
1024 Romagnoli, C., Santos, R., 2020. Bedforms on the submarine flanks of insular
1025 volcanoes: New insights gained from high-resolution seafloor surveys.
1026 Sedimentology 2020, https://doi.org/10.1111/sed.12725.
1027 Cesca, S., Letort, J., Razafindrakoto, H.N.T., Heimann, S., Rivalta, E., Isken, M.P.,
1028 Nikkhoo, M., Passarelli, L., Petersen, G.M., Cotton, F., Dahm, T., 2020. Drainage of
1029 a deep magma reservoir near Mayotte inferred from seismicity and deformation.
1030 Nature Geoscience, Vol 13, p 87–93.
1031 Chiocci, F. L., Casalbore, D., 2017, Unexpected fast rate of morphological evolution of
1032 geologically-active continental margins during Quaternary: Examples from selected
1033 areas in the Italian seas, Marine and Petroleum Geology, 82, 154-162. doi:
1034 10.1016/j.marpetgeo.2017.01.025
1035 Chiocci, F. L., Romagnoli, C., Casalbore, D., Sposato, A., Martorelli, E., Alonso, B., ... &
1036 Estrada, F., 2013. Bathy-morphological setting of Terceira Island (Azores) after the
1037 FAIVI cruise. Journal of Maps, 9(4), 590-595.
1038 Chorowicz, J., 2005. The East African Rift System. Journal of African Earth Sciences 43
1039 (1–3): 379–410. https://doi.org/10.1016/j.jafrearsci.2005.07.019.
1040 Clague, D.A., Paduan, J.B., Caress, D.W., Moyer, C.L., Glazer, B.T., Yoerger, D.R.,
1041 2019. Structure of Lō‘ihi Seamount, Hawai‘i and Lava Flow Morphology From High-
1042 Resolution Mapping. Front. Earth Sci. 7:58.doi: 10.3389/feart.2019.00058.

1043 Clague, D.A., Moore, J.G., Reynolds, J.R. 2000. Formation of submarine flat-topped
1044 volcanic cones in Hawai'i, Research article, Bull. Volcanol (2000) 62:214-233
1045 Clare, M.A., Le Bas, T., Price, D.M., Hunt, J.E., Sear, D., Cartigny, M.J.B., Vellinga, A.,
1046 Symons, W., Firth, C., Cronin, S., 2018. Complex and cascading triggering of
1047 submarine landslides and turbidity currents at Mvolcanic Islands revealed from
1048 mintegration of high-resolution onshore and offshore surveys. Frontiers Earth Sci.,
1049 6, 223.
1050 Clark, J.D., Kenyon, N.H., Pickering, K.T., 1992. Quantitative analysis of the geometry of
1051 submarine channels: implications for the classification of submarine fans. Geology
1052 20, 633–636.
1053 Class, C., Goldstein, S.L., Altherr, R., Bachèlery, P. 1998. The process of plume–
1054 lithosphere interactions in the ocean basins—the case of Grande Comore. J Petrol
1055 39 (5):881–903.
1056 Coffin, M. F., Rabinowitz, P.D., 1987. Reconstruction of Madagascar and Africa:
1057 evidence from the Davie fracture zone and western Somali basin. Journal of
1058 Geophysical Research-Solid Earth and Planets 92 (B9): 9385–9406.
1059 https://doi.org/10.1029/JB092iB09p09385.
1060 Connor, C.B., and Conway, F.M., 2000, Basaltic volcanic fields, in Sigurdsson, H., ed.,
1061 Encyclopedia of Volcanoes: San Diego, California, Academic Press, p. 331–343.
1062 Coombs, M.L., Clague, D.A., Moore, G.F., Cousens, B.L., 2004. The growth and
1063 collapse of Waianae volcano, Hawaii, as revealed by exploration of its submarine
1064 flanks. Geochem. Geophys. Geosyst. Vol 5, N 8. doi:10.1029/2004GC000717.
1065 Correggiari, A., Trincardi, F., Langone, L., Roveri, M., 2001. Styles of failure in heavily
1066 sedimented highstand prodelta wedges on the Adriatic shelf. J. Sediment. Res. 71,
1067 218 – 236

1068 Counts, J. W., Jorry, S. J., Leroux, E., Miramontes, E., Jouet, G., 2018. Sedimentation
1069 adjacent to atolls and volcano-cored carbonate platforms in the Mozambique
1070 Channel (SW Indian Ocean). Marine Geology 404, 41-59.
1071 Courgeon, S., Bachèlery, P., Jouet, G., Jorry, S.J., Bou, E., BouDagher-Fadel, M.K.,
1072 Révillon, S., Camoin, G., Poli, E., 2018. The offshore east African rift system: new
1073 insights from the Sakalaves seamounts (Davie Ridge, SW Indian Ocean). Terra
1074 Nova, 30, 5, 380-388, DOI: 10.1111/ter.12353.
1075 Darwin, C.R., 1842. The structure and distribution of coral reefs. Being the first part of
1076 the geology of the voyage of the Beagle, under the command of Capt. Fitzroy, R.N.
1077 during the years 1832 to 1836. London: Smith Elder and Co.
1078 Davis, J.K., Lawver, L.A., Norton, I.O., Gahagan, L.M., 2016. New Somali Basin
1079 magnetic anomalies and a plate model for the early Indian Ocean. Gondwana
1080 Research 34, 16–28. https://doi.org/10.1016/j.gr.2016.02.010.
1081 Debeuf, D., 2004. Etude de l'évolution volcano-structurale et magmatique de Mayotte
1082 (Archipel des Comores, Océan Indien): Approches structurale, pétrographique,
1083 géochimique et géochronologique. Unpublished Ph. D. thesis, Université de La
1084 Réunion, 243 pp
1085 Debeuf, D., 2011. Etude de l'évolution volcano-structurale et magmatique de Mayotte,
1086 Archipel des Comores, Océan Indien : approches structurale, pétrographique,
1087 géochimique et géochronologique. Volcanologie. Université de la Réunion, 2009.
1088 Français.
1089 Denlinger, R.P., Morgan, J.K., 2014. Instability of Hawaiian volcanoes. In: Poland, M.P.,
1090 Takahashi, T.J., Landowski, Claire M., C.M. (Eds.), Characteristics of Hawaiian
1091 Volcanoes Professional Paper 1801. U.S. Geological Survey, Reston, VA, USA, pp.
1092 149–176.

1093 Deville, E., Marsset, T., Courgeon, S., Jatiault, R., Ponte, J.P., Thereau, E., Jouet, G.,
1094 Jorry, S.J., Droz, L., 2018. Active fault system across the oceanic lithosphere of the
1095 Mozambique Channel: implications for the Nubia–Somalia southern plate boundary.
1096 Earth Planet. Sci. Lett. 502. https://doi.org/10.1016/j.epsl.2018.08.052.
1097 Devey, C.W., Lackschewitz, K.S., Mertz, D.F., Bourdon, B., Cheminee, J-L., Dubois, J.,
1098 Guivel, C., Hekinian, R., Stoffers, P., 2003. Giving birth to hotspot volcanoes :
1099 Distribution and composition of young seamounts from the seafloor near Tahiti and
1100 Pitcairn islands. Geology, v. 31; no. 5; p. 395–398.
1101 Dieterich, J. H., 1988. Growth and persistence of Hawaiian volcanic rift zones. Journal of
1102 Geophysical Research: Solid Earth, 93 (B5), 4258-4270.
1103 Duffield, W.A., Bacon, C.R., Dalrympe, G.B., 1980, Late Cenozoic volcanism,
1104 geochronology, and structure of the Coso Range, Inyo County, California, Journal of
1105 Geophysical Research, vol.85, p.2381-2404.
1106 Dullo, W.C., Camoin, G.F., Blomeier, D., Colonna, M., Eisenhauer, A., Faure, G.,
1107 Casanova, J., Thomassin, B.A., 1998. Morphology and sediments of the fore-slopes
1108 of Mayotte, Comoros Islands: direct observations from a submersible. Specialized
1109 Publication of the International Association of Sedimentologists 25, 219–236.
1110 Emerick, C.M., 1985. Age progressive volcanism in the Comores Archipelago and
1111 northern Madagascar. PhD thesis, Oregon State University, 195 pp.
1112 Emerick, C.M., Duncan, R.A., 1982. Age Progressive Volcanism in the Comores
1113 Archipelago, Western Indian Ocean and Implications for Somali Plate Tectonics.
1114 Earth and Planetary Science Letters 60 (3): 415–428.
1115 Emmel, B., Kumar, R., Ueda, K., Jacobs, J., Daszinnies, M.C., Thomas, R.J., Matola, R.,
1116 2011. Thermochronological history of an orogen-passive margin system: An

example from northern Mozambique. Tectonics 30, TC2002. doi:10.1029/2010TC002714.

Esson, J., Flower, M.F.J., Strong, D.F., Upton, B.G.J., Wadsworth, W.J., 1970. Geology of the Comores Archipelago, Western Indian Ocean, Geological Magazine 107 (06): 549–557.

Famin, V., Michon, L., Bourhane, A., 2020. The Comoros archipelago: A right-lateral transform boundary between the Somalia and Lwandle plates, Tectonophysics, https://doi.org/10.1016/j.tecto.2020.228539.

Feuillet, N., Jorry, S.J., Crawford, W., Deplus, C., et al., 2019. Birth of a large volcano offshore Mayotte through lithosphere-scale rifting. AGU Fall Meeting, V52D-01, San Francisco.

Franke, D., Jokat, W., Ladage, S., Stollhofen, H., Klimke, J., Lutz, R., Mahanjane, E.S., Ehrhardt, A., Schreckenberger, B., 2015. The Offshore East African Rift System: Structural Framework at the Toe of a Juvenile Rift. Tectonics 34 (10): 2015TC003922. https://doi.org/10.1002/2015TC003922.

Gaffney, E.S., Damjanac, B., and Valentine, G.A., 2007, Localization of volcanic activity: 2. Effects of preexisting structure: Earth and Planetary Science Letters, v. 263, p. 323–338, doi:10.1016/j.epsl.2007.09.002.

Gee, M.J.R., Masson, D.G.,Watts, A.B., Mitchell, N.C., 2001. Passage of debris flows and turbidity currents through a topographic constriction: seafloor erosion and deflection of pathways. Sedimentology 48, 1389–1409.

Geist, D. J., D. J. Fornari, M. D. Kurz, K. S. Harpp, S. Adam Soule, M. R. Perfit, and A. M. Koleszar. 2006. Submarine Fernandina: Magmatism at the leading edge of the Galápagos hot spot, Geochem. Geophys. Geosyst., 7, Q12007, doi:10.1029/2006GC001290.

1142 Geyer, A. and Martí, J., 2010, The Distribution of Basaltic Volcanism on Tenerife, Canary
1143 Islands: Implications on the Origin and Dynamics of the Rift Systems.
1144 Tectonophysics, 483, 310-326. http://dx.doi.org/10.1016/j.tecto.2009.11.002
1145 Guilcher, A., Berthois, L., Le Calvez, Y., Battistini, R., Crosnier, A., 1965. Les récifs
1146 coralliens et le lagon de l'île de Mayotte, Arch. Des Comores, Océan Indien. Mém.
1147 ORSTOM, n°11, 211pp.
1148 Hajash, A., Armstrong, R.L., 1972. Paleomagnetic and Radiometric Evidence for the Age
1149 of the Comores Islands, West Central Indian Ocean. Earth and Planetary Science
1150 Letters 16 (2): 231–36., https://doi.org/10.1016/0012-821X(72)90195-1.
1151 Hekinian, R., Cheminée, J.-L., Dubois, J., Stoffers, P., Scott, S., Guivel, C., Garbe-
1152 Schönberg, D., Devey, C., Bourdon, B., Lackschewitz, K., McMurtry, G., and Le
1153 Drezen, E., 2003. The Pitcairn hotspot in the South Pacific: Distribution and
1154 composition of submarine volcanic sequences, Journal of Volcanology and
1155 Geothermal Research, 121, 219-245. https://doi.org/10.1016/S0377-0273(02)00427-
1156 4.
1157 Holcomb, R.T., Searle R.C., 1991. Large landslides from oceanic volcanoes, Mar.
1158 Geotechnol., 10 (1-2), 19-32, doi: 10.1080/10641199109379880.
1159 Huff W.D., Owen, L.A., 2013. Volcanic landforms and hazards. In: John F. Shroder
1160 (Editor-in-chief), Owen, L.A. (Volume Editor). In Treatise on Geomorphology, Vol 5,
1161 Tectonic Geomorphology, San Diego: Academic Press, pp. 148–192.
1162 Hunt, J. E., Talling, P. J., Clare, M. A. & Jarvis, I., 2014. Long-term (17 Ma) turbidite
1163 record of the timing and frequency of large flank collapses of the Canary Islands.
1164 Geochem. Geophys. Geosyst. 15, 3322–3345 (2014).

1165 Hunt, J.E., Jarvis, I. 2017. Prodigious submarine landslides during the inception and
1166 early growth of volcanic islands. Nat Commun 8, 2061 (2017).
1167 https://doi.org/10.1038/s41467-017-02100-3
1168 Key, R.M., Smith, R.A., Smelror, M., Sæther, O.M., Thorsnes, T., Powell, J.H., Njange,
1169 F., Zandamela, E.B., 2008. Revised lithostratigraphy of the Mesozoic-Cenozoic
1170 succession of the onshore Rovuma Basin, northern coastal Mozambique. South Afr.
1171 J. Geol. 111, 89–108. doi:10.2113/gssajg.111.1.89.
1172 Krastel, S., Schmincke, H.U., Jacobs, C.L., Rihm R, Le Bas, T., M., Alibés, B., 2001a.
1173 Submarine landslides around the Canary Islands. J. Geoph. Res. 106(B3): 3977–
1174 3997.
1175 Krastel, S., Schmincke, H.U., Jacobs, C.L., 2001b. Formation of submarine canyons on
1176 the flanks of the Canary Islands. Geo-Marine Letters, 20: 160-167, DOI
1177 10.1007/s003670000049.
1178 Kusky, T.M., Toraman, E., Raharimahefa, T., Rasoazanamparany, C., 2010. Active
1179 tectonics of the Alaotra–Ankay Graben System, Madagascar: Possible extension of
1180 Somalian–African diffusive plate boundary? Gondwana Research 18, 274–294.
1181 https://doi.org/10.1016/j.gr.2010.02.003.
1182 Lachassagne, P., Aunay, B., Frissant, N., Guilbert, M., Malard, A., 2014. High-resolution
1183 conceptual hydrogeological model of complex basaltic volcanic islands: a Mayotte,
1184 Comoros, case study. Terra Nova, 26, 307–321, doi: 10.1111/ter.12102.
1185 Lacquement, F., Nehlig, P., Bernard, J., 2013. Carte géologique de Mayotte. BRGM,
1186 Report RP-61803-FR.
1187 Le Friant, A., Lebas, E., Clément, V., Boudon, G., Deplus, C., de Voogd, B., Bachèlery,
1188 P., 2011. A new model for the evolution of La Réunion volcanic complex from

complete marine geophysical surveys. Geophysical Research Letters, 38, L09312. https://doi.org/10.1029/2011GL047489.

Lee, H.J., Syvitski, J.P.M., Parker, G., Orange, D., Locat, J., Hutton, E.W.H. and Imran, J., 2002. Distinguishing sediment waves from slope failure deposits: field examples, including the “Humboldt Slide” and modeling results. Mar. Geol., 192, 79-104

Lemoine, A., Briole, P., Bertil, D., Roullé, A., Foumelis, M., Thinon, I., Raucoules, D., de Michele, M., Valty, P., Hoste Colomer, R., 2020. The 2018–2019 seismo-volcanic crisis east of Mayotte, Comoros islands: seismicity and ground deformation markers of an exceptional submarine eruption. Geophys. J. Int., 223, 22–44.

Lénat, J.F., Bachèlery, P., Merle, O.,2012. Anatomy of Piton de la Fournaise Volcano (La Réunion, Indian Ocean), Bulletin of Volcanology 74(9):1945-1961, DOI: 10.1007/s00445-012-0640-y

Leroux, E., Counts, J., Jorry, S., Jouet, G., Révillon, S., BouDagher-Fadel, M.K., Courgeon, S., Berthod, C., Ruffet, G., Bachèlery, P., Grenard-Grand, E., 2020. Evolution of the Glorieuses seamount in the SW Indian ocean and surrounding deep Somali basin since the Cretaceous, Marine Geology 427 (2020) 106202, https://doi.org/10.1016/j.margeo.2020.106202

MacDonald, G.A., 1972. Volcanoes. Prentice-Hall, Englewood Cliffs, NJ

Macgregor, D., 2015. History of the development of the East African Rift System: a series of interpreted maps through time. Journal of African Earth Sciences 101, 232–252.

Malod, J.A., Mougenot, D., Raillard, S., Maillard, A., 1991. New constraints on the kinematics of madagascar - tectonic structures of the Davie ridge. Comptes Rendus Academie des Sciences, Serie II, 312 (13): 1639–46.

1213 Masson, D.G., Watts, A.B., Gee, M.J.R., Urgeles, R., Mitchell, N.C., Le Bas, T.P.,
1214 Canals, M., 2002. Slope failures on the flanks of the western Canary Islands. Earth
1215 Science Reviews 57: 1–35.
1216 Masson, D.G., Le Bas, T.P., Grevemeyer, I., Weinrebe, W., 2008. Flank collapse and
1217 large-scale landsliding in the Cape Verde Islands, off West Africa Masson,
1218 Geochem. Geophys. Geosyst., 9, Q07015. doi:10.1029/2008GC001983.
1219 Mazuel, A., Sisavath, E., Babonneau, N., Jorry, S.J., Bachèlery, P., Delacourt, C., 2016.
1220 Turbidity current activity along the flanks of a volcanic edifice: The Mafate
1221 volcaniclastic complex, La Réunion Island, Indian Ocean. Sedimentary Geology,
1222 Elsevier, 2016, 335, pp.34 - 50.
1223 McGuire, W. J., 1996. Volcano instability: A review of contemporary themes. Geological
1224 Society, London, Special Publications, 110(1), 1–23.
1225 https://doi.org/10.1144/GSL.SP.1996.110.01.01.
1226 Medialdea, T., Somoza, L., Gonzalez, F.J., Vazquez, J.T., de Ignacio, C., Sumino, H.,
1227 Sanchez-Guillamón, O., Orihashi, Y., Leon, R., Palomino, D., 2017. Evidence of a
1228 modern deep water magmatic hydrothermal system in the Canary Basin (eastern
1229 central Atlantic Ocean), Geochem. Geophys. Geosyst., 18, 3138– 3164,
1230 doi:10.1002/2017GC006889.
1231 Micallef, A. and Mountjoy, J.J., 2011. A topographic signature of a hydrodynamic origin
1232 for submarine gullies. Geology, 39, 115–118.
1233 Michon, L., 2016. The Volcanism of the Comoros Archipelago Integrated at a Regional
1234 Scale. In Active Volcanoes of the Southwest Indian Ocean, edited by Patrick
1235 Bachèlery, Jean-François Lénat, Andrea Di Muro, and Laurent Michon, 333–44.
1236 Berlin, Heidelberg: Springer Berlin Heidelberg. https://doi.org/10.1007/978-3-642-
1237 31395-0_21.

1238 Mitchell, N.C., 2001. The transition from circular to stellate forms of submarine
1239 volcanoes, J. Geophys. Res., Vol 106, p. 1987– 2003, 2001.
1240 Mitchell, N.C., Masson, D.G., Watts, A.B., Gee, M.J., Urgeles, R., 2002. The morphology
1241 of the submarine flanks of volcanic ocean islands: A comparative study of the
1242 Canary and Hawaiian hotspot islands. J. Volcanol. Geotherm. Res. 115:83-107.
1243 Mitchell, N. C., 2003. Susceptibility of mid-ocean ridge volcanic islands and seamounts
1244 to large-scale landsliding. J. Geophys. Res. Solid Earth 108, 1–14.
1245 Mitchell, N.C., Strect, R., Oppenheimer, C., Kay, D., Beier, C., 2012. Cone morphology
1246 associated with shallow marine eruptions: east Pico Island, Azores. Bull. Volcanol.
1247 74, 2289–2301.
1248 Mitchell, N.C., Quartau, R., Madeira, J., 2013. Large-scale active slump of the
1249 southeastern flank of Pico Island, Azores: Comment, Geology, 41(12), e301.
1250 Montaggioni, L. F., Martin-Garin, B., 2020. Quaternary development history of coral reefs
1251 from West Indian islands: a review. International Journal of Earth Sciences, 1-20.
1252 Moore, J.G., 1964. Giant submarine landslides on the Hawaiian Ridge. in Geological
1253 Survey Research: U.S. Geol. Survey Prof. Paper 501-D, p. D95-D98.
1254 Moore, J.G., Fiske R.S., 1969. Volcanic substructure inferred from dredge samples and
1255 ocean-bottom photographs, Hawaii. Geological Society of America Bulletin 80 (7):
1256 1191-1202.
1257 Moore, J.G., Clague, D.A., Holcomb, R.T., Lipman, P.W., Normark, W.R., Torresan,
1258 M.E., 1989. Prodigious submarine landslides on the Hawaiian ridge, J. Geophys.
1259 Res., 94, 17,465–17, 484.
1260 Moore, J. G., Normark, W. R. & Holcomb, R. T. 1994. Giant Hawaiian landslides. Annu.
1261 Rev. Earth Planet. Sci. 22, 119–144 (1994).

1262 Morgan, W.J., 1972. Deep mantle convection: plumes and plate motions. Am Ass
1263 Petroleum Geol Bull 56:203-213.
1264 Morgan, J. K., G. F. Moore, and D. A. Clague, 2003. Slope failure and volcanic
1265 spreading along the submarine south flank of Kilauea volcano, Hawaii, J. Geophys.
1266 Res., 108(B9), 2415, doi:10.1029/2003JB002411.
1267 Mougenot, D., Recq, M., Virlogeux, P., Lepvrier, C., 1986. Seaward extension of the
1268 East-African Rift. Nature 321 (6070): 599–603. https://doi.org/10.1038/321599a0.
1269 Mpanda, S., 1997. Geological development of the East African coastal basin of
1270 Tanzania.
1271 Mueller, C.O., Jokat, W., 2019. The initial Gondwana break-up; A synthesis based on
1272 new potential field data of the Africa-Antarctica corridor. Tectonophysics, 750, 301-
1273 328.
1274 Muffler, L.J.P., Clynne, M.A., Calvert, A.T., Champion, D.E., 2011. Diverse, discrete,
1275 mantle-derived batches of basalt erupted along a short normal fault zone : The
1276 poison Lake chain, southernmost Cascades, Geological Society of America Bulletin
1277 123(11-12):2177-2200, DOI: 10.1130/b30370.1
1278 Mulder, T., 2011. (4.2.3) Depositional bedforms: Sediment waves, In : Deep-Sea
1279 Sediments, Developments in Sedimentology, Vol 63, 2011, Pages 715-764, Edited
1280 by Heiko HüNeke, Thierry Mulder, https://doi.org/10.1016/B978-0-444-53000-4.00010-
1281 X
1282 Nehlig, P., Lacquement, F., Bernard, J., Caroff, M., Deparis, J., Jaouen, T., Pelleter, A.,
1283 Perrin, J., Prognon, C., Vittecoq, B., 2013. Notice de la carte géologique de Mayotte
1284 BRGM/RP-61803-FR, 143pp, 45 fig., 1 ann.
1285 Németh, K., Kereszturi, G., 2015. Monogenetic volcanism: personal views and
1286 discussion. International Journal of Earth Sciences, 104, 2131–2146.

1287 Neves, M.C., Miranda, J.M., Luis, J.F., 2013. The role of lithospheric processes on the
1288 development of linear volcanic ridges in the Azores. Tectonophysics 608, 376–388.
1289 Nougier, J., Cantagrel, J.M., Karche, J. P. 1986. The Comores Archipelago in the
1290 Western Indian Ocean: Volcanology, Geochronology and Geodynamic Setting.
1291 Journal of African Earth Sciences (1983) 5 (2): 135–44.
1292 https://doi.org/10.1016/0899-5362(86)90003-5.
1293 O'Connor, J.M., Jokat, W., Regelous, M. et al., 2019. Superplume mantle tracked
1294 isotopically the length of Africa from the Indian Ocean to the Red Sea. Nat Commun
1295 10, 5493. https://doi.org/10.1038/s41467-019-13181-7
1296 Oehler, J.F., Lénat, J.F., Labazuy, P., 2008. Growth and collapse of the Reunion Island
1297 volcanoes, Bull Volcanol (2008) 70:717–742, DOI 10.1007/s00445-007-0163-0.
1298 Paquet, F., Jorry, S., Deplus, C., Le Friant, A., Julien, B., Bremell-Fleury, S., Feuillet, N.,
1299 Gaillot, A., Guérin, C., Thinon, I., 2019. The Mayotte Seismo-volcanic crisis:
1300 characterizing a reactivated volcanic ridge from the upper slope to the abyssal plain
1301 using multibeam bathymetry and backscatter data, in Proceedings of the AGU Fall
1302 Meeting 2019. AGU.
1303 Pelleter, A.A., Caroff, M., Cordier, C., Bachèlery, P., Nehlig, P., Debeuf, D., Arnaud, N.,
1304 2014. Melilite-bearing lavas in Mayotte (France): An insight into the mantle source
1305 below the Comores. Lithos, n° 208–209, 281–297,
1306 http://dx.doi.org/10.1016/j.lithos.2014.09.012.
1307 Postma, G., Cartigny, M., 2014, Supercritical and subcritical turbidity currents and their
1308 deposits- a synthesis. Geology 42:987–990
1309 Puga-Bernabéu, A., Webster, J.M., Braga, J.C., Clague, D.A., Dutton, A., Eggins, S.,
1310 Fallon, S., Jacobsen, G., Paduan, J.B., Potts, D.C. 2016. Morphology and evolution

of drowned carbonate terraces during the last two interglacial cycles, off Hilo, NE Hawaii. Marine Geology, 371, 57-81, https://doi.org/10.1016/j.margeo.2015.10.016

Quartau, R., Trenhaile, A.S., Mitchell, N.C. and Tempera, F. 2010. Development of volcanic insular shelves: insights from observations and modelling of Faial Island in the Azores Archipelago. Mar. Geol., 275, 66 –83

Quartau, R., Hipólito, A., Romagnoli, C., Casalbore, D., Madeira, J., Tempera, F., ... & Chiocci, F. L. 2014. The morphology of insular shelves as a key for understanding the geological evolution of volcanic islands: insights from Terceira Island (Azores). Geochemistry, Geophysics, Geosystems, 15(5), 1801-1826.

Raillard, S., 1990. Les marges de l'Afrique de l'est et les zones de fracture associées. Chaine Davie et Ride du Mozambique. Campagne MD-60/MACAMO-1I, Thèse d'Université Univ. P. et M. Curie, Paris, 272p.

Ramalho, R.S., Quartau, R., Trenhaile, A.S., Mitchell, N.C., Woodroffe, C.D., Ávila, S.P., 2013. Coastal evolution on volcanic oceanic islands: A complex interplay between volcanism, erosion, sedimentation, sea-level change and biogenic production. Earth Science Reviews 127 (2013) 140-170. https://doi.org/10.1016/j.earscirev.2013.10.007.

Rindraharisaona, E. J., Guidarelli, M., Aoudia, A., Rambolamanana, G., 2013. Earth structure and instrumental of Madagascar: implications on the seismotectonics. Tectonophysics 594:165–181. doi:10.1016/j.tecto. 2013.03.033.

Ricchi, A., Quartau, R., Ramalho, R.S., Romagnoli, C., Casalbore, D., Ventura da Cruz, J., Fradique, C., Vinhas, A., 2018, Marine terrace development on reefless volcanic islands: New insights from high-resolution marine geophysical data offshore Santa Maria Island (Azores Archipelago), Marine Geology, vol. 406, p.42-56, https://doi.org/10.1016/j.margeo.2018.09.002

1336 Ricchi, A., Quartau, R., Ramalho, R.S., Romagnoli, C., Casalbore, D., Zhao, Z., 2020,
1337 Imprints of volcanic, erosional, depositional, tectonic and mass-wasting processes in
1338 the morphology of Santa Maria insular shelf (Azores), Marine Geology, Volume
1339 424, June 2020, https://doi.org/10.1016/j.margeo.2020.106163
1340 Romagnoli, C., Casalbore, D., Chiocci, F.L., Bosman, A., 2009. Off-shore evidence of
1341 large-scale lateral collapses on the eastern flank of Stromboli, Italy, due to
1342 structurally-controlled, bilateral flank instability, Mar. Geol., 262,1–13,
1343 doi:10.1016/j.margeo.2009.02.004.
1344 Romagnoli, C., 2013. Characteristics and morphological evolution of the Aeolian
1345 volcanoes from the study of submarine portions. In: Lucchi, F., Peccerillo, A., Keller,
1346 J., Tranne, C.A., Rossi, P.L. (Eds.), The Aeolian Islands Volcanoes. Geological
1347 Society, London, Memoirs, 37, 13-26.
1348 Romagnoli, C., Casalbore, D., Bosman, A., Braga, R., & Chiocci, F. L., 2013. Submarine
1349 structure of Vulcano volcano (Aeolian Islands) revealed by high-resolution
1350 bathymetry and seismo-acoustic data. Marine Geology, 338, 30-45.
1351 Romagnoli, C., Casalbore, D., Ricchi, A., Lucchi, F., Quartau, R., Bosman, A., ... &
1352 Chiocci, F. L. 2018. Morpho-bathymetric and seismo-stratigraphic analysis of the
1353 insular shelf of Salina (Aeolian archipelago) to unveil its Late-Quaternary geological
1354 evolution. Marine Geology, 395, 133-151.
1355 Romagnoli, C., Belvisi, V., Innangi, S., Di Martino, G., Tonielli, R. 2020. New insights on
1356 the evolution of the Linosa volcano (Sicily Channel) from the study of its submarine
1357 portions, «MARINE GEOLOGY», 2020, 419, pp. 1 – 12
1358 Romero Ruiz, C., García-Cacho, L., Araña, V., Yanes Luque, A., Felpeto, A., 2000.
1359 Submarine volcanism surrounding Tenerife, Canary Islands: implications for tectonic

1360 controls, and oceanic shield forming processes. J. Volcanol. Geotherm. Res. 103,
1361 105–119.
1362 Rubin, K.H., Soule, S.A., Chadwick Jr., W.W., Fornari, D.J., Clague, D.A., Embley, R.W.,
1363 Baker, E.T., Perfit, M.R., Caress, D.W., Dziak, R.P., 2012. Volcanic eruptions in the
1364 deep sea. Oceanography 25(1):142–157,
1365 http://dx.doi.org/10.5670/oceanog.2012.12.
1366 Saint-Ange, F., Bachèlery, P., Babonneau, N., Michon, L., Jorry, S.J., 2013.
1367 Volcaniclastic sedimentation on the submarine slopes of a basaltic hotspot volcano:
1368 Piton de la Fournaise volcano (La Réunion Island, Indian Ocean). Mar Geol 337:35–
1369 52. doi:10.1016/j.margeo.2013.01.004.
1370 Sanchez-Guillamón, O., Vázquez, J.,T., Palomino, D., Medialdea, T., Fernández-Salas,
1371 L., M., León, R., Somoza, L., 2018. Morphology and shallow structure of seafloor
1372 mounds in the Canary Basin (Eastern Central Atlantic Ocean), Geomorphology 313
1373 (2018) 27–47.
1374 Schlager, W. and Camber, O., 1986. Submarine slope angles, drowning unconformities,
1375 and self-erosion of limestone escarpments. Geology, 14, 762–765.
1376 Segoufin, J., Patriat, P., 1980. Existences d'anomalies mésozoïques dans le bassin de
1377 Somalie : Implications pour les relations Afrique-Antarctique-Madagascar, C.R.
1378 Acad. Sci., 291, 85-88, 1980.
1379 Shom, 2016. MNT Bathymétrique de façade de Mayotte (Projet Homonim).
1380 http://dx.doi.org/10.17183/MNT_MAY100m_HOMONIM_WGS84
1381 Sisavath, E., Babonneau, N., Saint-Ange, F., Bachèlery, P., Jorry, S.J., Deplus, C., de
1382 Voogd, B., Savoye, B., 2011. Morphology and sedimentary architecture of a modern
1383 volcaniclastic turbidite system: The Cilaos fan, offshore La Réunion Island, Marine

1384 Geology, Volume 288, Ticket 1-4, p.1-17 (2011), DOI:
1385 10.1016/j.margeo.2011.06.011.
1386 Smith, I. E. M., Németh, K. 2017. Source to surface model of monogenetic volcanism: a
1387 critical review, Geological Society, London, Special Publications, 446, 1-28, 31
1388 March 2017, https://doi.org/10.1144/SP446.14
1389 Späth, A., LeRoex, A.P., Duncan, R.A., 1996. The Geochemistry of Lavas from the
1390 Comores Archipelago, Western Indian Ocean: Petrogenesis and Mantle Source
1391 Region Characteristics. Journal of Petrology 37 (4): 961–91.
1392 https://doi.org/10.1093/petrology/37.4.961.
1393 Spiess, F.N., Luyendyk, B.P., Larson, R.L., Normark, W.R., Mudie, J.D., 1969. Detailed
1394 geophysical studies on the northern Hawaiian Arch using a deeply towed instrument
1395 package. Marine Geology 7(6), pp. 501-527.
1396 Stamps, D.S., Saria, E., Kreemer, C., 2018. A Geodetic Strain Rate Model for the East
1397 African Rift System. Sci. Rep.8, 732. https://doi.org /10.1038 /s41598-017-19097-w.
1398 Staudigel, H., Koppers, A.A.P., 2015. Seamounts and island building. In: Sigurdsson, H.,
1399 Houghton, B., McNutt, S., Rymer, H., Stix, J. (Eds.), The Encyclopedia of
1400 Volcanoes, 2nd Edition Academic Press, pp. 405–422.
1401 Stretch, R.C., Mitchell, N., Portaro, R.A., 2006. A morphometric analysis of the
1402 submarine volcanic ridge south-east of Pico Island, Azores, in Journal of
1403 Volcanology and Geothermal Research 156(1):35-54, DOI:
1404 10.1016/j.jvolgeores.2006.03.009
1405 Thompson, J.O., Moulin, M., Aslanian, D., de Clarens, P., Guillocheau, F., 2019. New
1406 starting point for the Indian Ocean: Second phase of breakup for Gondwana. Earth-
1407 Science Reviews, 1991,26-56, https://doi.org/10.1016/j.earscirev.2019.01.018.

1408 Tilling, R. I., Dvorak, J. J., 1993. Anatomy of a basaltic volcano. Nature, 363 (6425), 125-
1409 133.
1410 Upton, B.G.J., 1982. Oceanic Islands. In: Nairn P, Stehli F (eds) Ocean basins and their
1411 margins, Indian Ocean, vol 6(13). Plenum Press, New York, pp 585–648.
1412 Valentine, G.A., and Krogh, K.E.C., 2006, Emplacement of shallow dikes and sills
1413 beneath a small basaltic volcanic center—The role of pre-existing structure (Paiute
1414 Ridge, southern Nevada, USA): Earth and Planetary Science Letters, v. 246, p.
1415 217–230, doi:10.1016/j.epsl.2006.04.031.
1416 Vittecoq, B., Deparis, J., Violette, S., Jaouën, T., Lacquement, F., 2014. Influence of
1417 successive phases of volcanic construction and erosion on Mayotte Island's
1418 hydrogeological functioning as determined from a helicopter-borne resistivity survey
1419 correlated with borehole geological and permeability data. Journal of Hydrology,
1420 509, 519-538.
1421 Wanless, V.D., Garcia, M.O., Trusdell, F.A., Rhodes, J.M., Norman, M.D., Weis, D.,
1422 2006. Submarine radial vents on Mauna Loa Volcano Hawai'i. Geochem. Geophys.
1423 Geosyst. Vol. 7, N° 5, 1-28, doi: 10.1029/2005GC001086.
1424 Weiß, B.J., Huebscher, C., Ludmann, T., 2015, The Tectonic Evolution of the South-
1425 Eastern Terceira Rift / São Miguel Region (Azores), Tectonophysics 654, DOI:
1426 10.1016/j.tecto.2015.04.018
1427 Wynn, R.B., Piper, D.J.W. and Gee, M.J.R. 2002. Generation and migration of coarse-
1428 grained sediment waves in turbidity current channels and channel–lobe transition
1429 zones. Mar. Geol., 192, 59 –78
1430 Zinke, J., Reijmer, J.J.G., Dullo, W.-Ch., Thomassin, B.A., 2003a. Systems tracts
1431 sedimentology in the lagoon of Mayotte associated with the Holocene transgression.
1432 Sed. Geol., 160, 57-79.

1433 Zinke, J., Reijmer, J.J.G., Thomassin, B.A., Dullo, W.-Chr., Grootes, P.M., Erlenkeuser,
1434 H., 2003b. Postglacial Flooding History of Mayotte Lagoon (Comoro Archipelago,
1435 Southwest Indian Ocean). Marine Geology 194 (3–4): 181–96.
1436 https://doi.org/10.1016/S0025-3227(02)00705-3.
1437 Zinke, J., Reijmer, J.J.G., Taviani, M., Dullo, W.-Chr., Thomassin, B.A., 2005. Facies
1438 and faunal assemblage changes in response to the Holocene transgression in the
1439 Holocene transgression in the Lagoon of Mayotte (Comoro Archipelago, SW Indian
1440 Ocean). Facies 50:391–408 DOI 10.1007/s10347-004-0040-7
1441

Caption of figures

Fig.1: (A) Location of the Comoros archipelago in the Mozambique Channel. (B) Bathymetry around the Comoros archipelago (sources: Gridded Bathymetry Chart of the Oceans - GEBCO 2008, MNT Shom). (C) Detailed view of the volcanic ridge between Grande Comore and Mohéli islands. (D) Detailed view of the volcanic ridge between Mohéli and Anjouan islands. (E) Detailed view of the volcanic ridge between Anjouan and Mayotte islands. (F) Topographic profile across the Comoros archipelago.

Fig.2: (A) Morpho-bathymetric map of Grande Comore and Vailheu Bank (see location in Fig.1B). Onshore rift zones and landslides are from Bachèlery et al. (2016). The location of the profiles across the bedform fields shown in Figure 9 is indicated. (B) 3D underwater visualization of the channels and volcanic cones at the northern tip of Grande Comore (C) 3D visualization of Vailheu Bank and volcanic ridge VR2. (D) Bathymetric profile showing from west to east, Vailheu Bank and Grande Comore (a to c).

Fig.3: (A) Morpho-bathymetric map of Mohéli (see location in Fig.1B). Two bathymetric profiles intersecting the terraces T2Moh (in orange) and T3Moh (in green) are shown. The location of the profiles across the bedform fields shown in Figure 9 is indicated. (B) Underwater 3D visualization of the submarine plateau and the terrace T3Moh. On T3Moh collapsed debris are visible. (C) 3D view of the volcanic ridge that connects the SE of Mohéli and Anjouan, characterized by a multitude of conical reliefs. (D) Bathymetric profile across the island including the insular shelf and the terrace T3Moh (a to d). (E) Bathymetric profile along the volcanic ridge VR4, between Mohéli and Anjouan (e-f).

Fig.4: (A) Morpho-bathymetric map of Anjouan (see location in Fig.1B). A bathymetric profile (d-e) across the volcanic ridge VR5 is shown. (B) Bathymetric profile (a to c) from NW to E of Anjouan.

Fig.5: (A) Morpho-bathymetric map of Mayotte and the Jumelles (see location in Fig.1B). Two bathymetric profiles intersecting the terraces T2May (in blue) and T3May (in red) are shown. The location of the profiles across the bedform fields shown in Figure 9 is indicated. (B) Underwater 3D visualization of the Jumelles volcanic ridges. (C) Underwater 3D visualization of the SW terrace T1May. (D) Bathymetric profile (a to d) from W to E of Mayotte.

Fig.6: 3D images showing the main structures recognized throughout the Comoros archipelago. The location of each image is shown in the central map. d.a.d: debris avalanche deposits.

Fig.7: (A) Slope map of the SW of Grande Comore, and location of the bathymetric profiles (in red) and associated slope gradients (in green) of some selected features: (B) Mound, (C) Pointy volcanic cone, (D) Flat-topped volcanic cone (E) Channels separated by irregular and chaotic surfaces. Several units shaping the area covered by debris avalanche deposits are shown (black dashed lines).

Fig.8: (A, B) Seismic profiles across volcanic cones and mounds north of the archipelago and southwest of the Jumelles volcanic ridges (see location on Fig. 6C). Different seismic facies have been observed, the most prevalent being a set of parallel, well-stratified reflectors interpreted as sedimentary continuous layers. At some instances, up-bending reflectors are identified on the seafloor and creating large

mounds. On the mounds normal faults affect de sedimentary units. At other instances, multiple but no well-defined overlapping hyperbolae, with a low amplitude and chaotic acoustic facies, appear along inclined slopes corresponding to a volcanic cone. At the foot of the cone small chaotic and semitransparent lens can be interpreted as small mass-wasting deposits. Forced folds are present around the volcanic cones and mounds resulting from the extensional and compressional regimes of the area. (C) Seismic profile across the Jumelles volcanic ridge showing an acoustic signature typical of volcanic cones.

Fig.9: Bathymetric profiles (in black) and slope gradients (in blue) along the profiles of some bedform fields identified off Grande Comore (profiles' location in Fig.2), Mohéli (profiles' location in Fig.3) and Mayotte (profiles' location in Fig.5).

Fig.10: (A) Bathymetric profiles along submarine constructional volcanic flanks off the Comorian Islands. Flanks show rectilinear shaped slopes characterized by many irregularities mainly corresponding to volcanic cones. In comparison to the other Islands, Mayotte has gentler slopes reflecting a significant spreading of the formations and a higher sediment cover. (B) Bathymetric profiles along flanks affected by landsliding. All profiles have an overall concave upwards shape. The slightly convex zone downslope may result from debris avalanche deposits accumulation. Vertical exaggeration is ~ 7:1. Profile locations and lengths are shown on the corresponding map on the right.

Fig.11: Characteristics of the volcanic cones and mounds around the Comoros archipelago (upper graph). Basal diameter vs. height of volcanic cones and mounds;

dashed lines indicate values of aspect ratio (height/diameter). The measured volcanic cones have basal diameters ranging from 300 to ~3000 m, and an average height of 120 m. Sixty-five large cones have heights greater than 300 m (15 are over 400 m high). Their aspect ratio is 0.15 in average, with a slightly higher aspect ratio (0.21) for the highest (over 300 m) volcanic cones. Mounds mostly have aspect ratios lower than 0.04, with basal diameter up to 5000 m and heights not exceeding 120 m. In the lower graph, volcanic cones for other volcanic islands are shown for comparison. The volcanic cones surrounding the Comorian Islands have great similarities with those observed in the Azores.

Fig.12: Synthesis map of the main structures recognized throughout the Comoros archipelago. The main structural, volcanic and sedimentary features identified throughout our morpho-bathymetric study are shown here, as well as data from the literature such as volcanic rift zones and landslide scars on land (Bachèlery et al., 2016; Famin et al., 2020), fractures affecting the island and the insular shelf of Mayotte (Audru et al., 2006) and focal mechanisms (CMT 1976-2017, Lemoine et al. 2019).

Table 1: Morphologic characteristics of the main landforms of the Comoros archipelago.

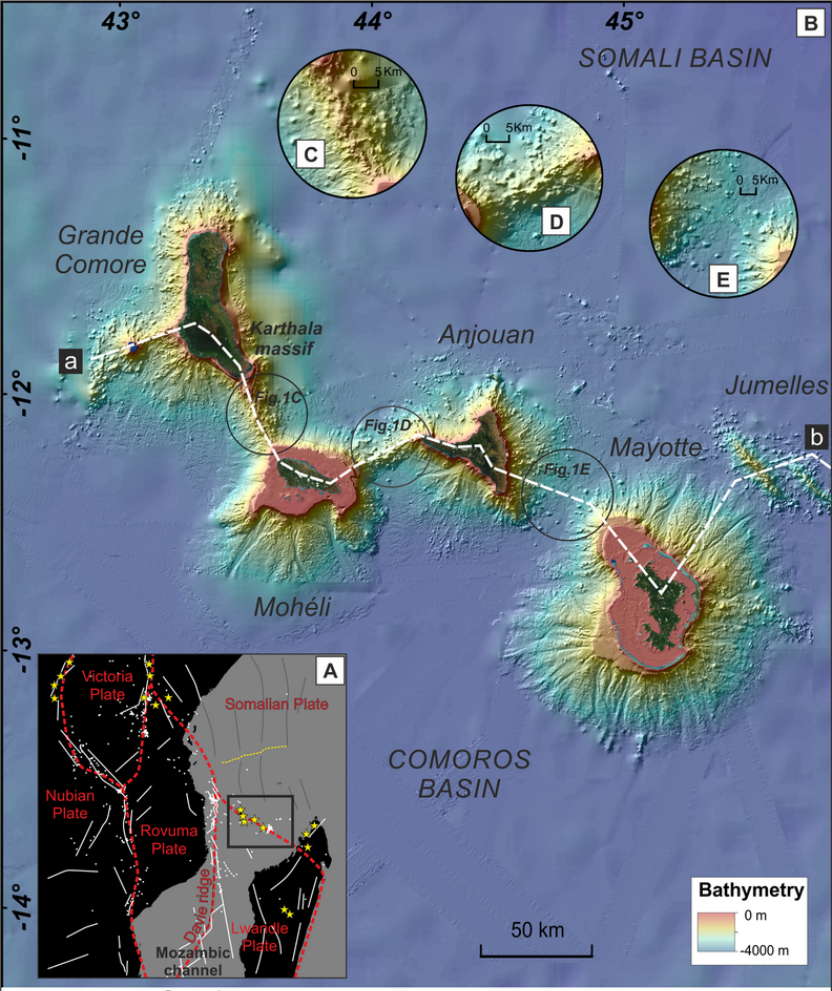
43°
44°
45°
B
SOMALI BASIN
-11°
-12°
-13°
-14°
0 5Km
C
D
E
Grande Comore
Karthala massif
Anjouan
Jumelles
Mayotte
a
b
Fig.1C
Fig.1D
Fig.1E
Mohéli
A
Victoria Plate
Somalian Plate
Nubian Plate
Rovuma Plate
Davie ridge
Lwandle Plate
Mozambic channel
COMOROS BASIN
50 km
Bathymetry
0 m
-4000 m

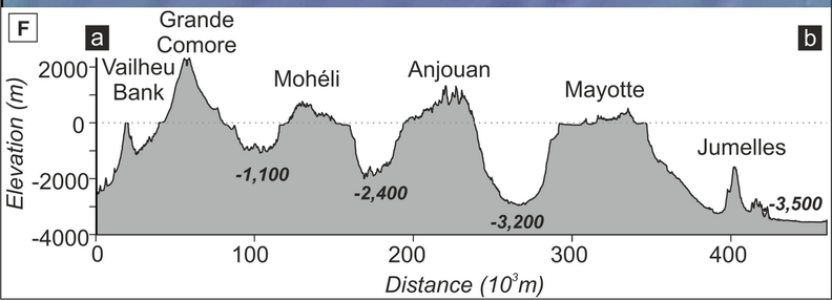
F
a
b
Grande Comore
Vailheu Bank
Mohéli
Anjouan
Mayotte
Jumelles
2000
0
-2000
-4000
Elevation (m)
-1,100
-2,400
-3,200
-3,500
0
100
200
300
400
Distance (10³m)

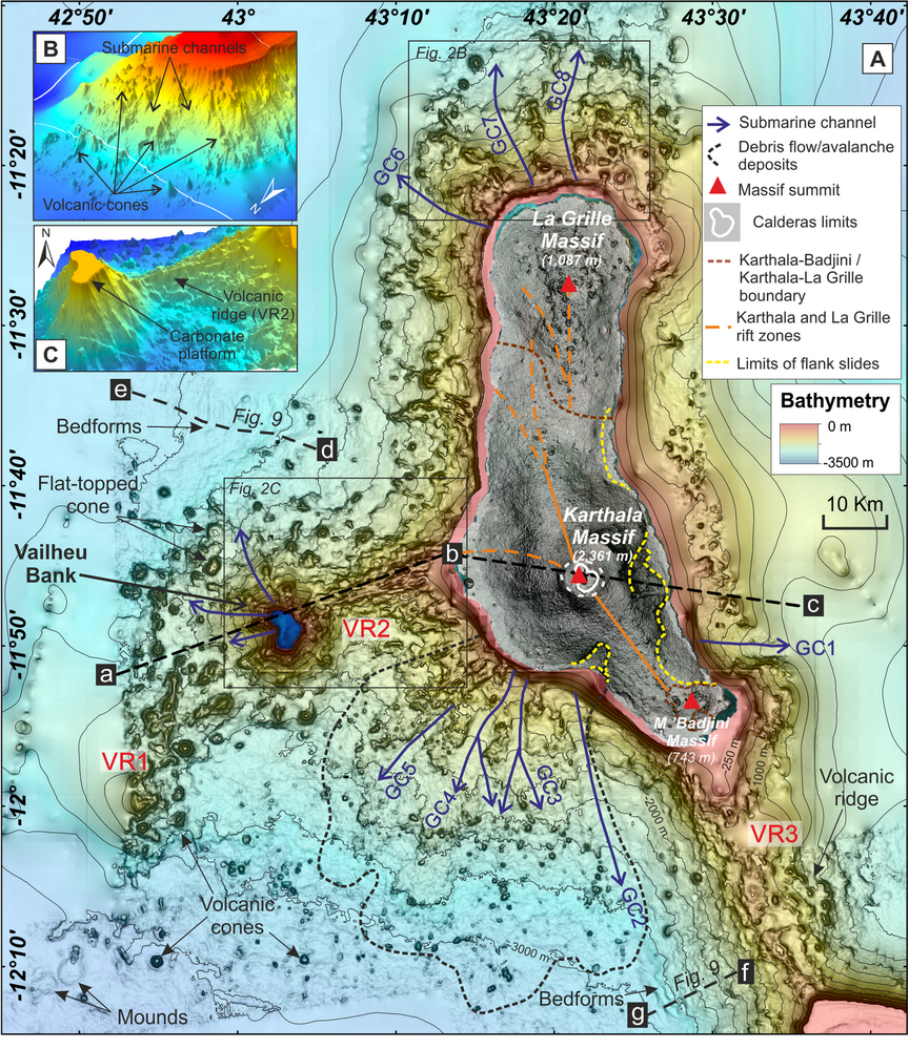
42°50'
43°
43°10'
43°20'
43°30'
43°40'
-11°20'
-11°30'
-11°40'
-11°50'
-12°
-12°10'
A
B
Submarine channels
Volcanic cones
C
N
Volcanic ridge (VR2)
Carbonate platform
Fig. 2B
Fig. 2C
Fig. 9
GC6
GC7
GC8
GC5
GC4
GC3
GC2
GC1
La Grille Massif (1,087 m)
Karthala Massif (2,361 m)
M'Badjini Massif (743 m)
Submarine channel
Debris flow/avalanche deposits
Massif summit
Calderas limits
Karthala-Badjini / Karthala-La Grille boundary
Karthala and La Grille rift zones
Limits of flank slides
Bathymetry
0 m
-3500 m
10 Km
Bedforms
Flat-topped cone
Vailheu Bank
VR1
VR2
VR3
Volcanic ridge
Volcanic cones
Mounds
250 m
1000 m
2000 m
3000 m
a
b
c
d
e
f
g

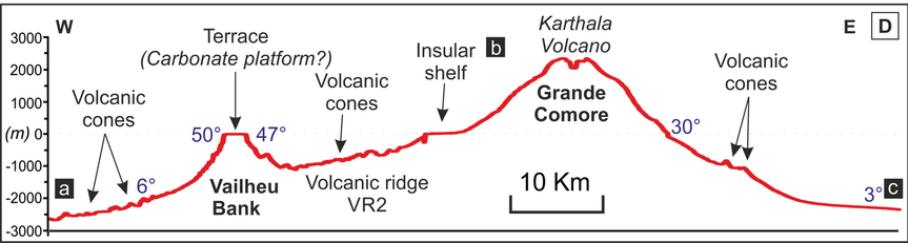
W
E
D
3000
2000
1000
(m) 0
-1000
-2000
-3000
Terrace (Carbonate platform?)
Volcanic cones
Volcanic cones
Insular shelf
b
Karthala Volcano
Grande Comore
Volcanic cones
50°
47°
30°
6°
3°
a
c
Vailheu Bank
Volcanic ridge VR2
10 Km

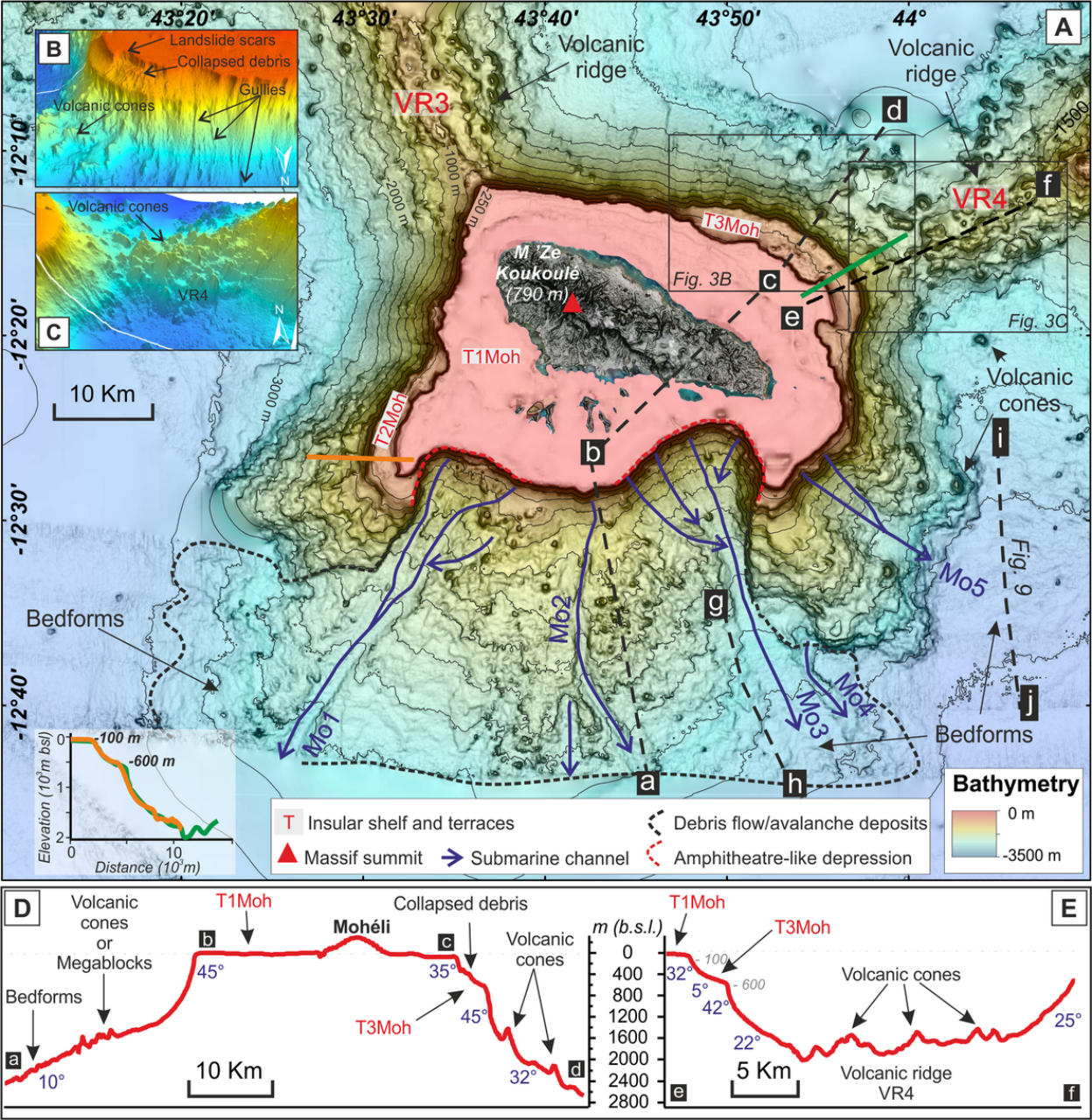
A
B
Landslide scars
Collapsed debris
Gullies
Volcanic cones
C
Volcanic cones
VR4
10 Km
43°20'
43°30'
43°40'
43°50'
44°
-12°10'
-12°20'
-12°30'
-12°40'
Volcanic ridge
Volcanic ridge
VR3
VR4
1000 m
2000 m
3000 m
1500
d
f
T3Moh
Fig. 3B
Fig. 3C
c
e
M 'Ze Koukoulé (790 m)
T1Moh
T2Moh
b
Volcanic cones
i
Fig. 9
Mo1
Mo2
Mo3
Mo4
Mo5
g
Bedforms
Bedforms
j
a
h
100 m
-600 m
Elevation (10³m bsl)
Distance (10³m)
T Insular shelf and terraces
Massif summit
Submarine channel
Debris flow/avalanche deposits
Amphitheatre-like depression
Bathymetry
0 m
-3500 m
D
Volcanic cones or Megablocks
T1Moh
Collapsed debris
Mohéli
Volcanic cones
Bedforms
b
c
45°
35°
45°
T3Moh
32°
a
10°
10 Km
d
m (b.s.l.)
0
400
800
1200
1600
2000
2400
2800
E
T1Moh
T3Moh
100
600
32°
5°
42°
22°
25°
Volcanic cones
5 Km
Volcanic ridge VR4
e
f

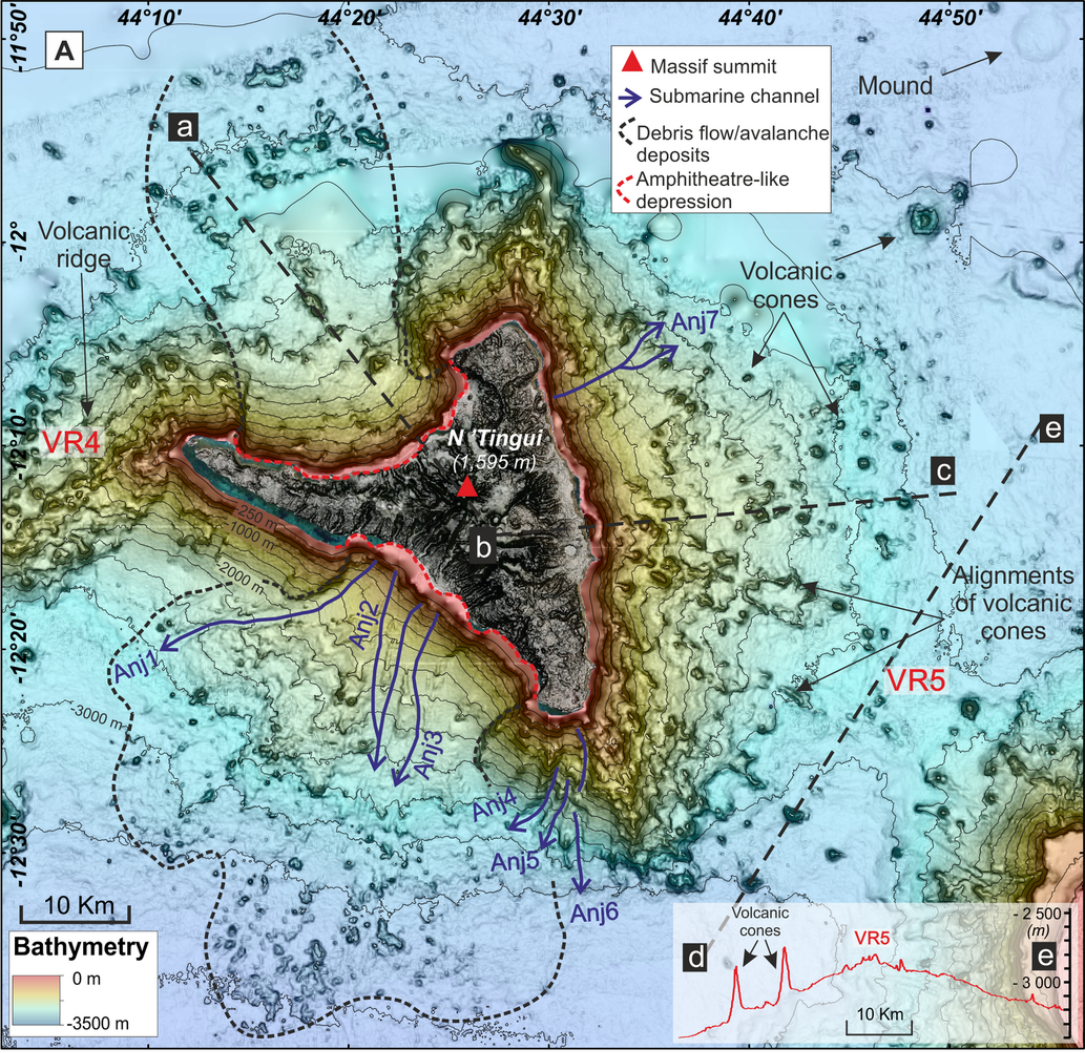
A
44°10'
44°20'
44°30'
44°40'
44°50'
-11°50'
-12°
-12°10'
-12°20'
-12°30'
Massif summit
Submarine channel
Debris flow/avalanche deposits
Amphitheatre-like depression
Mound
Volcanic ridge
Volcanic cones
Alignments of volcanic cones
VR4
VR5
N'Tingui
(1,595 m)
a
b
c
d
e
Anj1
Anj2
Anj3
Anj4
Anj5
Anj6
Anj7
-250 m
-1000 m
-2000 m
-3000 m
10 Km
Bathymetry
0 m
-3500 m
- 2 500 (m)
- 3 000
10 Km

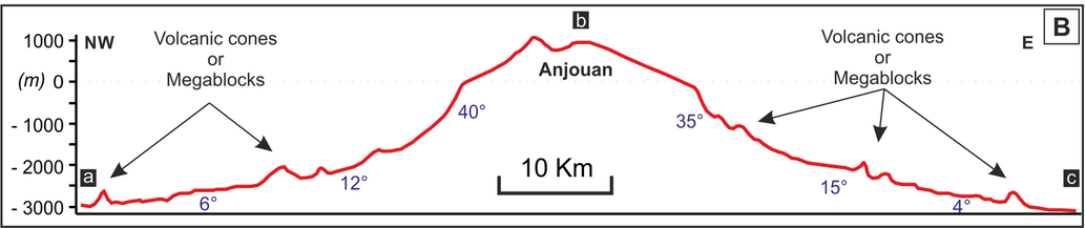
B
NW
E
1000
(m) 0
- 1000
- 2000
- 3000
Volcanic cones or Megablocks
Anjouan
Volcanic cones or Megablocks
6°
12°
40°
35°
15°
4°
10 Km

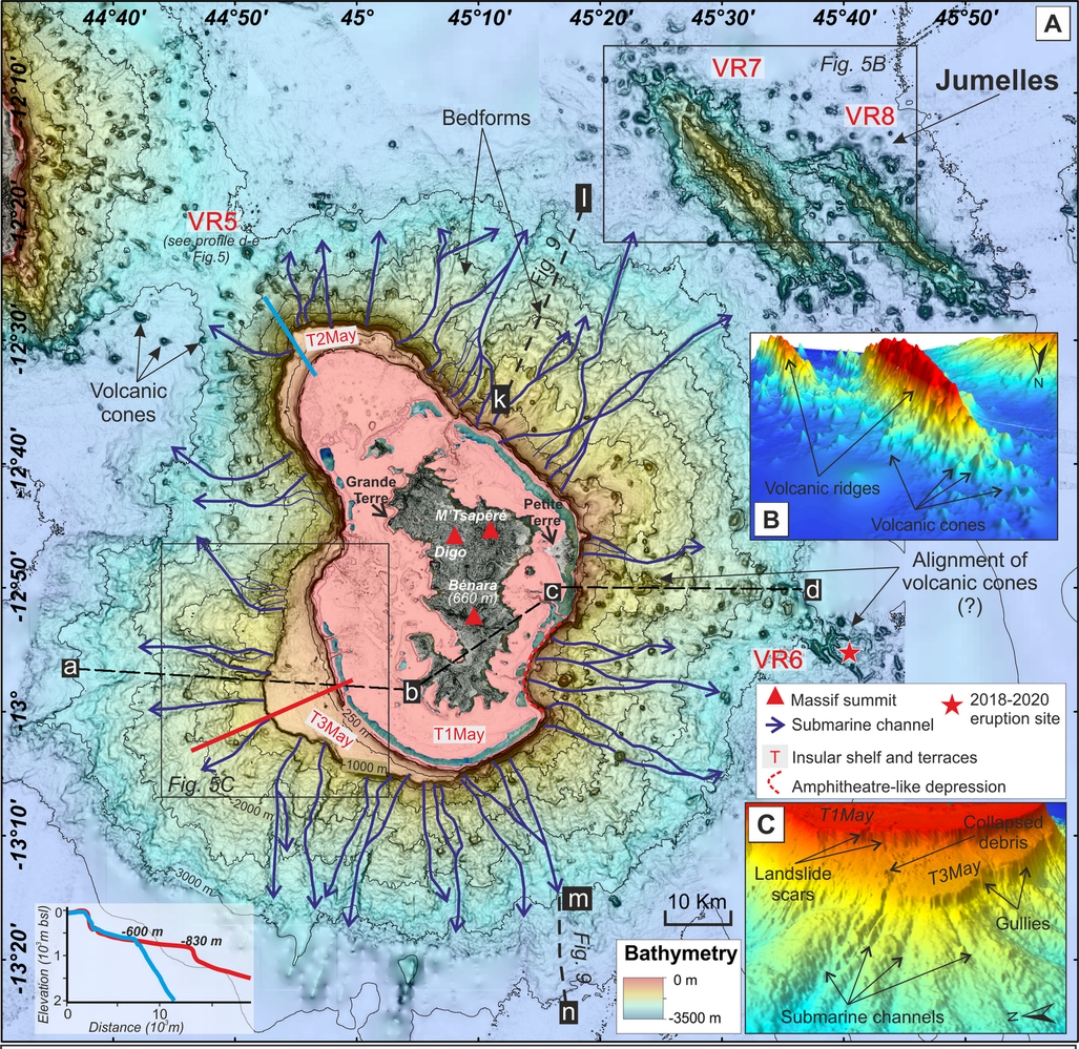
A
44°40'
44°50'
45°
45°10'
45°20'
45°30'
45°40'
45°50'
-12°10'
-12°20'
-12°30'
-12°40'
-12°50'
-13°
-13°10'
-13°20'
VR7
Fig. 5B
Jumelles
VR8
Bedforms
VR5
(see profile d-e Fig.5)
Fig. 6
Volcanic cones
T2May
k
l
Grande Terre
M'Tsapéré
Petite Terre
Digo
Bénara (660 m)
B
Volcanic ridges
Volcanic cones
N
Alignment of volcanic cones (?)
c
d
a
b
VR6
T3May
T1May
250 m
1000 m
2000 m
3000 m
Fig. 5C
Massif summit
2018-2020 eruption site
Submarine channel
Insular shelf and terraces
Amphitheatre-like depression
C
T1May
Collapsed debris
Landslide scars
T3May
Gullies
Submarine channels
N
m
n
Fig. 9
10 Km
Bathymetry
0 m
-3500 m
-600 m
-830 m
Elevation (10³ m bsl)
Distance (10³m)
D
W
E
(m bsl) 0
500
1000
1500
2000
2500
3000
Collapsed debris
T1May
Volcanic cones alignments
Submarine channel
Bedforms
T3May
- 830
Mayotte
10°
25°
34°
2-4°
44°
40°
25°
10°
10 Km

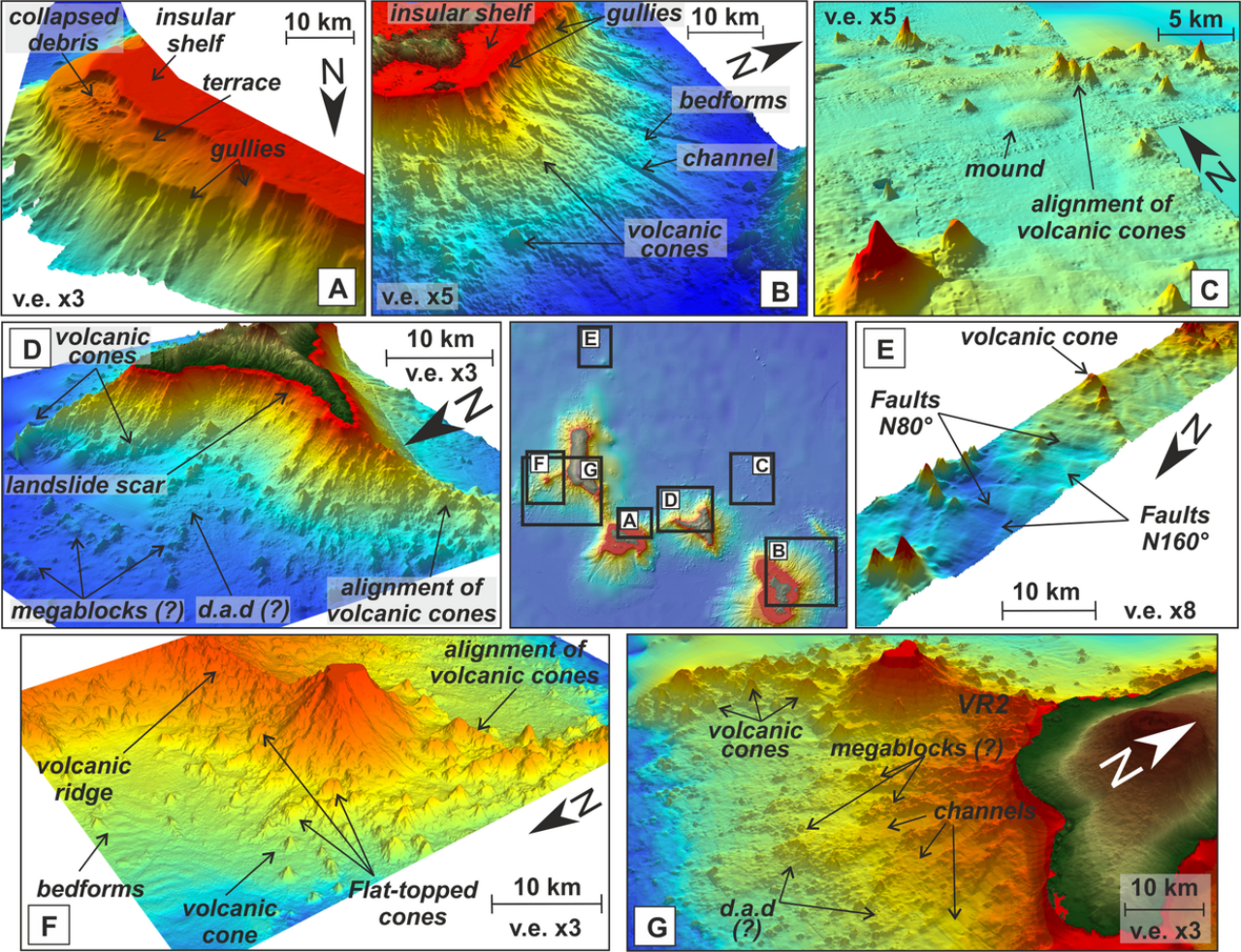
collapsed debris
insular shelf
terrace
gullies
10 km
N
v.e. x3
A
insular shelf
gullies
10 km
bedforms
channel
volcanic cones
v.e. x5
B
v.e. x5
5 km
mound
alignment of volcanic cones
C
D
volcanic cones
10 km
v.e. x3
landslide scar
megablocks (?)
d.a.d (?)
alignment of volcanic cones
E
F
G
A
D
C
B
E
volcanic cone
Faults N80°
Faults N160°
10 km
v.e. x8
alignment of volcanic cones
volcanic ridge
bedforms
volcanic cone
Flat-topped cones
10 km
v.e. x3
F
volcanic cones
VR2
megablocks (?)
channels
d.a.d (?)
10 km
v.e. x3
G

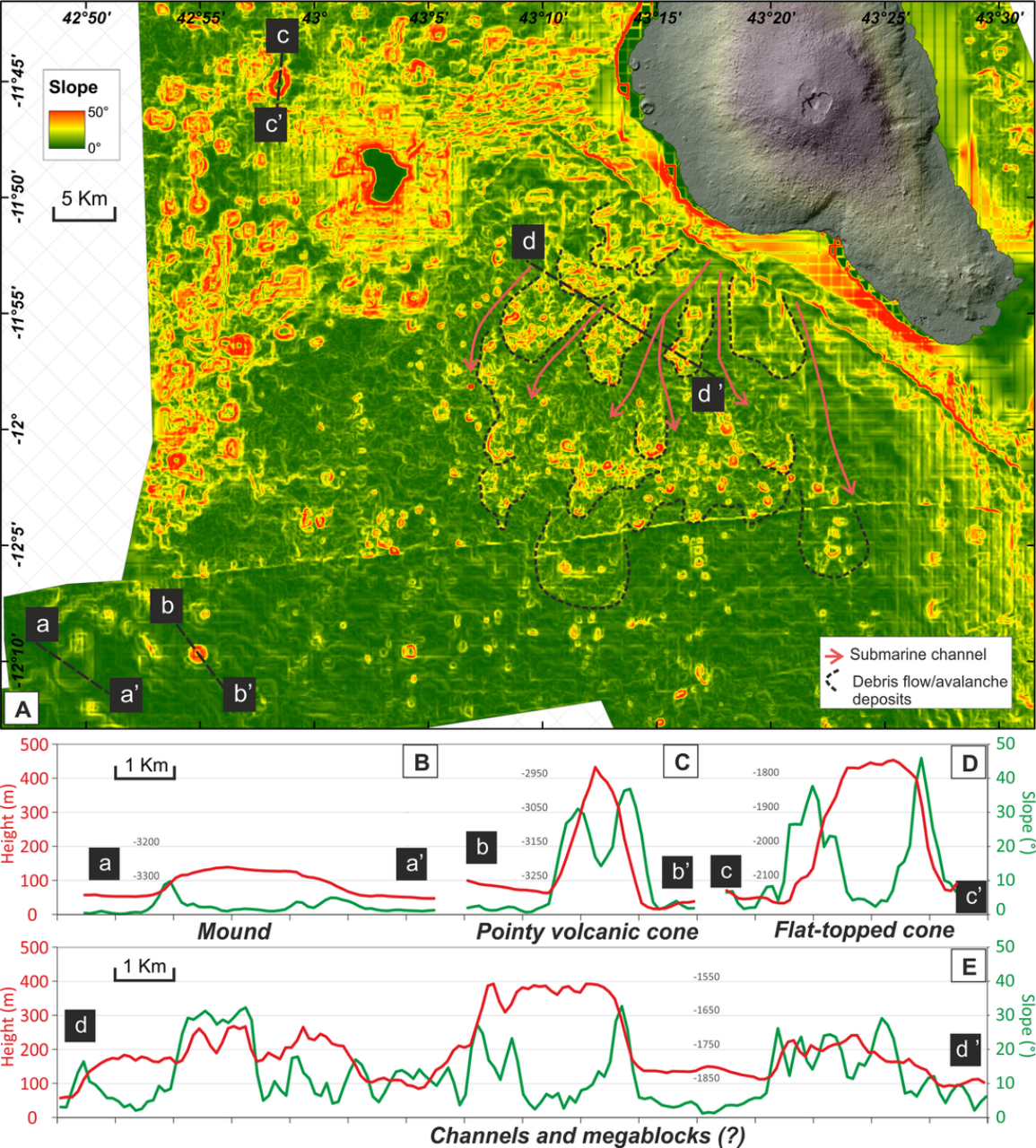
42°50'
42°55'
43°
43°5'
43°10'
43°15'
43°20'
43°25'
43°30'
-11°45'
-11°50'
-11°55'
-12°
-12°5'
-12°10'
Slope
50°
0°
5 Km
c
c'
d
d'
a
a'
b
b'
A
Submarine channel
Debris flow/avalanche deposits
1 Km
B
C
D
E
Height (m)
Slope (°)
Mound
Pointy volcanic cone
Flat-topped cone
Channels and megablocks (?)

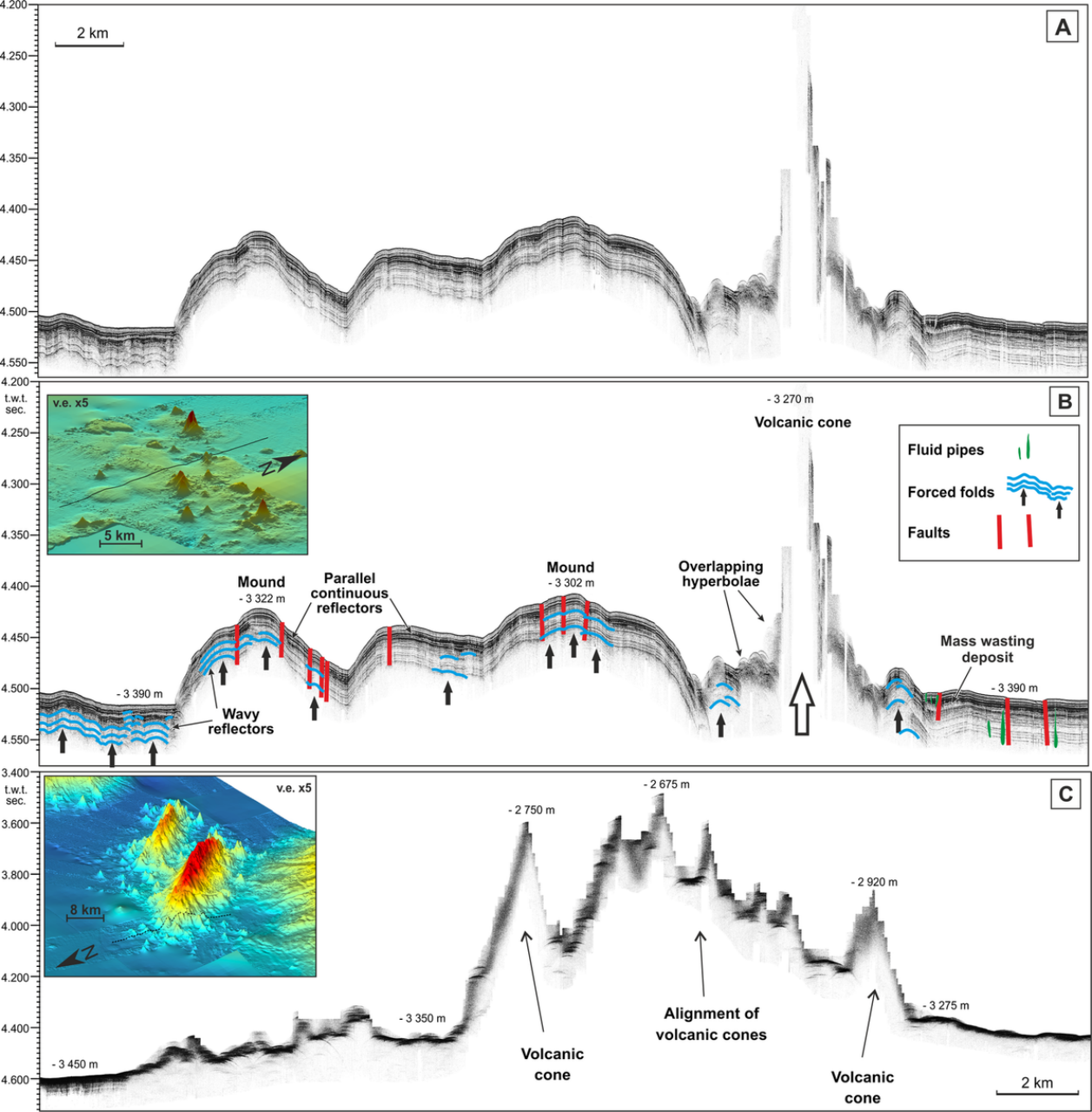
A
2 km
B
t.w.t. sec.
v.e. x5
5 km
- 3 270 m
Volcanic cone
Fluid pipes
Forced folds
Faults
Mound
- 3 322 m
Parallel continuous reflectors
Mound
- 3 302 m
Overlapping hyperbolae
Mass wasting deposit
- 3 390 m
- 3 390 m
Wavy reflectors
C
t.w.t. sec.
v.e. x5
8 km
- 2 750 m
- 2 675 m
- 2 920 m
- 3 350 m
- 3 275 m
- 3 450 m
Volcanic cone
Alignment of volcanic cones
Volcanic cone
2 km

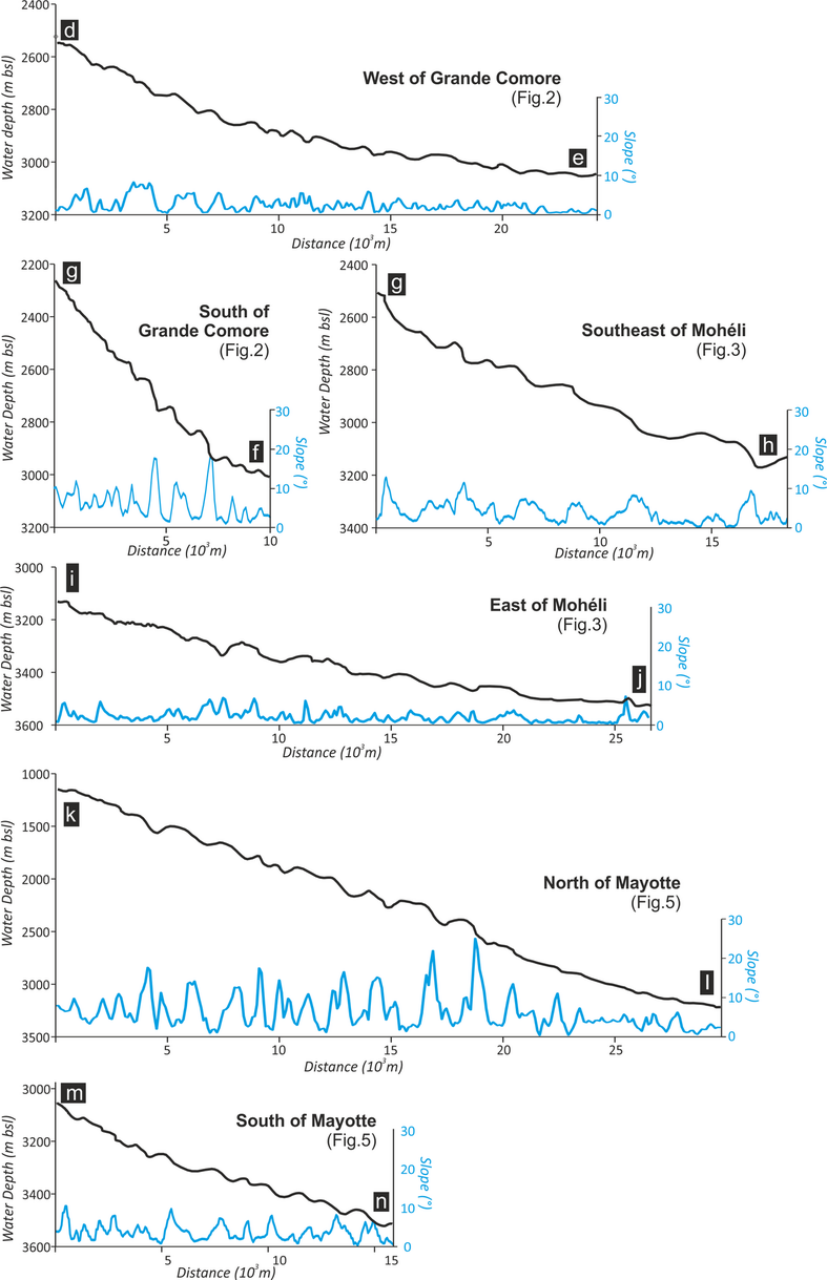
d
West of Grande Comore
(Fig.2)
e
Water depth (m bsl)
Slope (°)
Distance (10³m)
g
South of
Grande Comore
(Fig.2)
f
Water Depth (m bsl)
Slope (°)
Distance (10³m)
g
Southeast of Mohéli
(Fig.3)
h
Water Depth (m bsl)
Slope (°)
Distance (10³m)
i
East of Mohéli
(Fig.3)
j
Water Depth (m bsl)
Slope (°)
Distance (10³m)
k
North of Mayotte
(Fig.5)
l
Water Depth (m bsl)
Slope (°)
Distance (10³m)
m
South of Mayotte
(Fig.5)
n
Water Depth (m bsl)
Slope (°)
Distance (10³m)

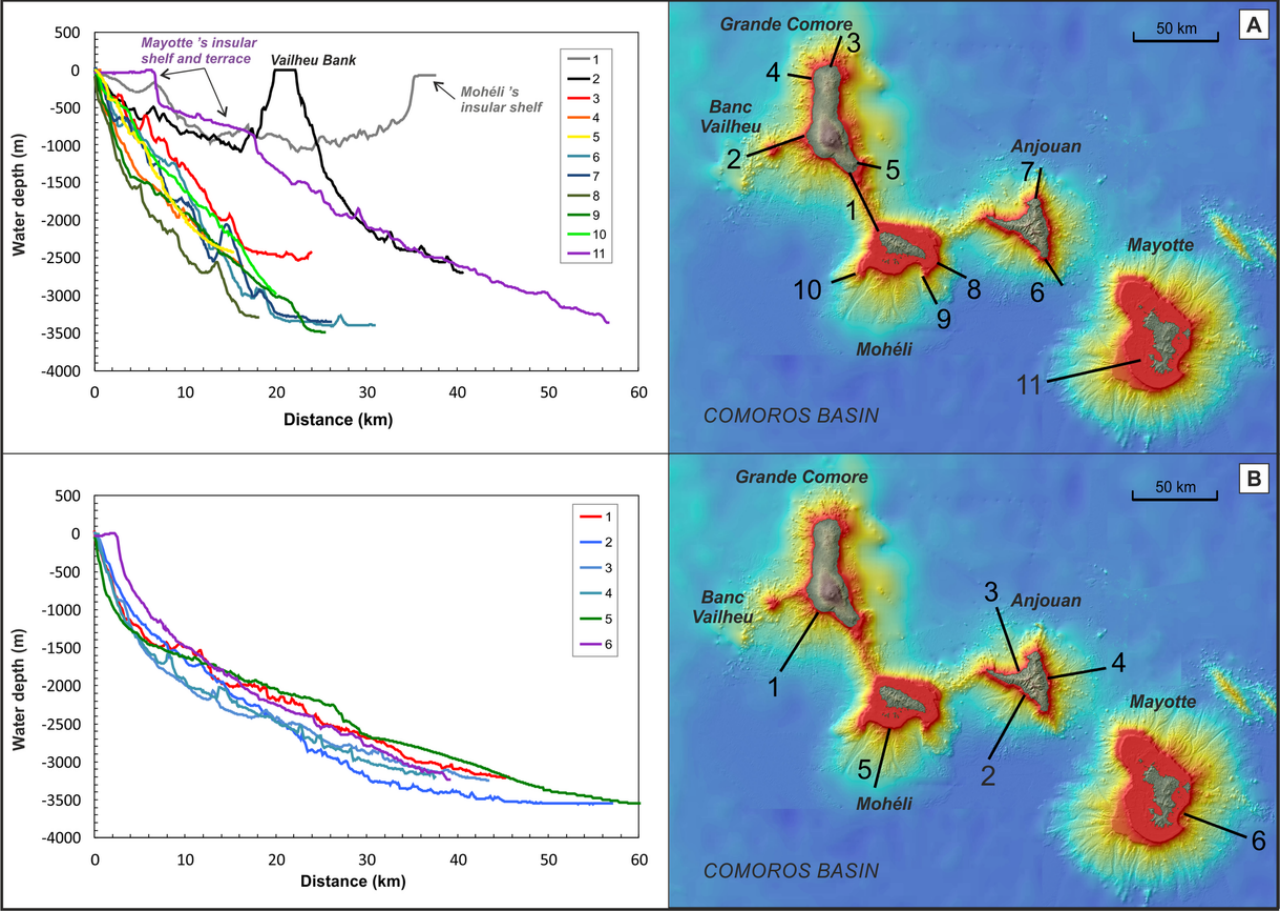
Mayotte 's insular shelf and terrace
Vailheu Bank
Mohéli 's insular shelf
Water depth (m)
Distance (km)
1
2
3
4
5
6
7
8
9
10
11
Grande Comore
Banc Vailheu
Anjouan
Mayotte
Mohéli
COMOROS BASIN
50 km
A
B

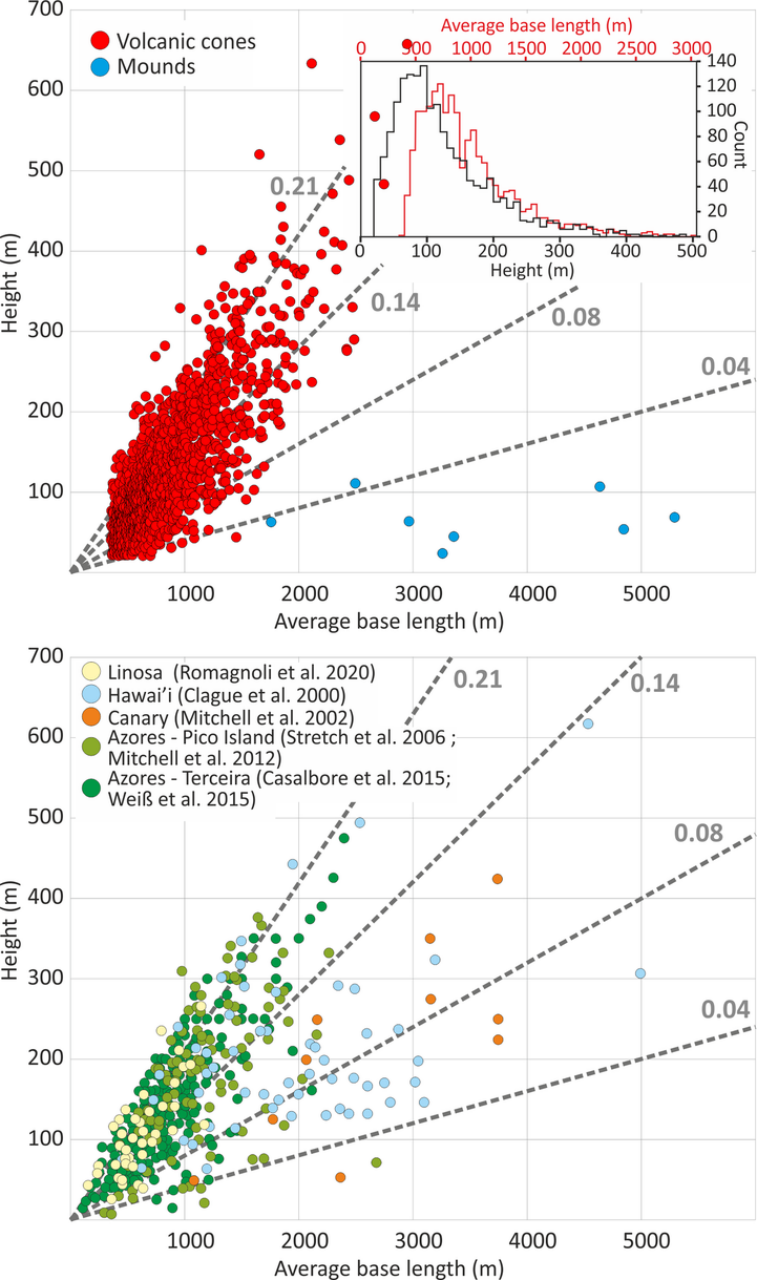
Volcanic cones
Mounds
Average base length (m)
0
500
1000
1500
2000
2500
3000
Count
Height (m)
0.21
0.14
0.08
0.04
Height (m)
Average base length (m)
Linosa (Romagnoli et al. 2020)
Hawai'i (Clague et al. 2000)
Canary (Mitchell et al. 2002)
Azores - Pico Island (Stretch et al. 2006 ; Mitchell et al. 2012)
Azores - Terceira (Casalbore et al. 2015; Weiß et al. 2015)
0.21
0.14
0.08
0.04
Height (m)
Average base length (m)

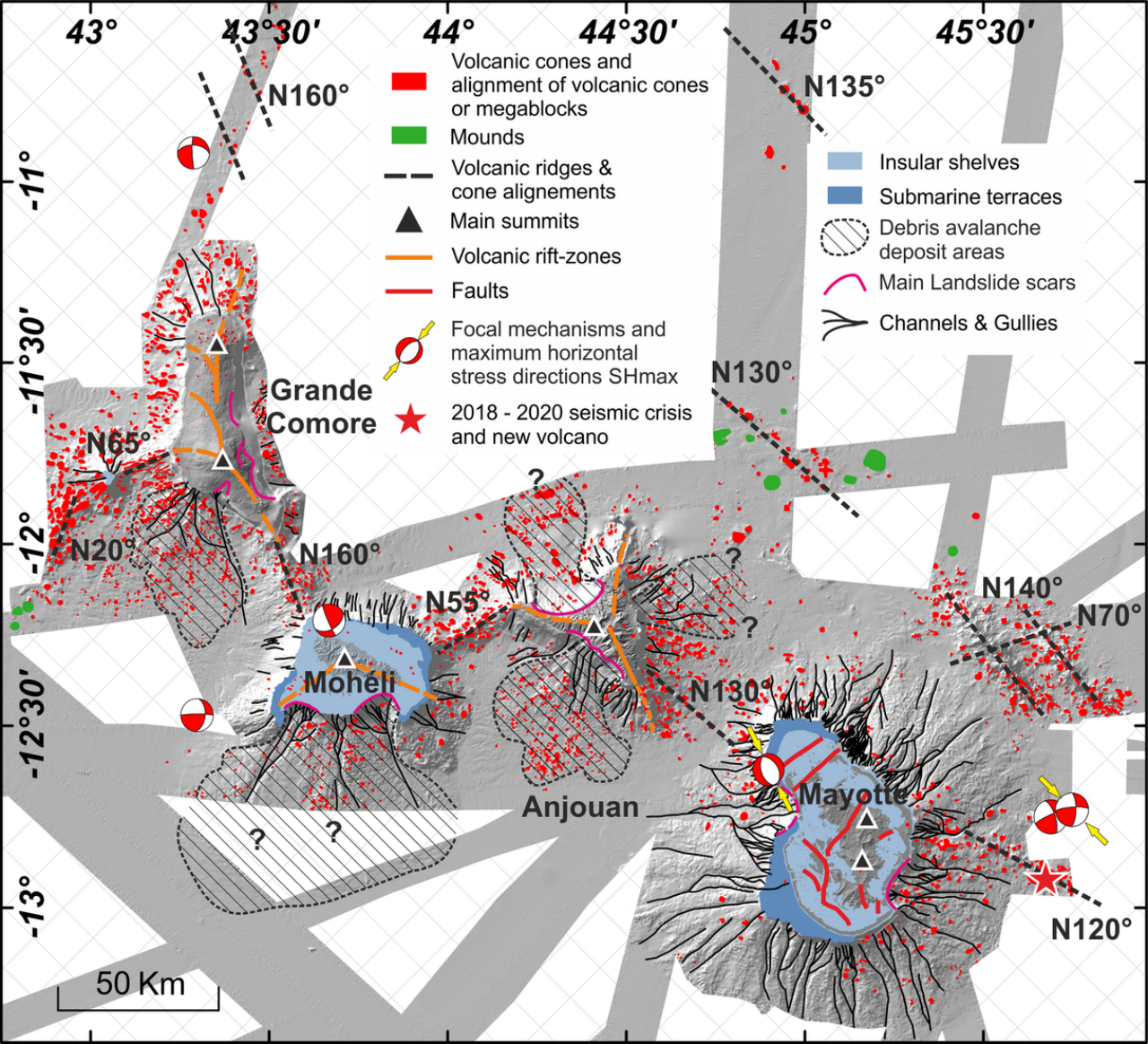
43°
43°30'
44°
44°30'
45°
45°30'
-11°
-11°30'
-12°
-12°30'
-13°
Volcanic cones and alignment of volcanic cones or megablocks
Mounds
Volcanic ridges & cone alignements
Main summits
Volcanic rift-zones
Faults
Focal mechanisms and maximum horizontal stress directions SHmax
2018 - 2020 seismic crisis and new volcano
Insular shelves
Submarine terraces
Debris avalanche deposit areas
Main Landslide scars
Channels & Gullies
N160°
N135°
N130°
N65°
N20°
N160°
N55°
N140°
N70°
N130°
N120°
Grande Comore
Moheli
Anjouan
Mayotte
?
50 Km